Annu. Rev. Fluid Mech. 1990. 22: 473–537

LOCAL AND GLOBAL INSTABILITIES IN SPATIALLY DEVELOPING FLOWS

Patrick Huerre[1]

Department of Aerospace Engineering, University of Southern California, Los Angeles, California 90089-1191

Peter A. Monkewitz

Department of Mechanical, Aerospace and Nuclear Engineering, University of California, Los Angeles, California 90024-1597

1. INTRODUCTION

The goal of this survey is to review recent developments in the hydrodynamic stability theory of *spatially developing flows* pertaining to absolute/convective and local/global instability concepts. We wish to demonstrate how these notions can be used effectively to obtain a qualitative and quantitative description of the spatio-temporal dynamics of open shear flows, such as mixing layers, jets, wakes, boundary layers, plane Poiseuille flow, etc.

In this review, we only consider *open flows* where fluid particles do not remain within the physical domain of interest but are advected through downstream flow boundaries. Thus, for the most part, flows in "boxes" (Rayleigh-Bénard convection in finite-size cells, Taylor-Couette flow between concentric rotating cylinders, etc.) are not discussed. Furthermore, the implications of local/global and absolute/convective instability concepts for geophysical flows are only alluded to briefly.

In many of the flows of interest here, the mean-velocity profile is non-

[1] Present address: Département de Mécanique, Ecole Polytechnique, 91128 Palaiseau Cedex, France.

0066–4189/90/0115–0473$02.00

uniform in the streamwise direction, and in order to distinguish between local and global instability properties, it is first essential to assume that streamwise variations of the mean flow are slow over a typical instability wavelength. The terms "*local*" and "*global*" then refer to the instability of the local velocity profile and of the entire flow field, respectively. At the local level of description, it is further necessary to characterize the impulse response of the system within the parallel-flow approximation at each streamwise station. If localized disturbances spread upstream and downstream and contaminate the entire parallel flow, the velocity profile is said to be *locally absolutely unstable*. If, by contrast, disturbances are swept away from the source, the velocity profile is said to be *locally convectively unstable*. One of the main objectives of recent theoretical efforts has thus been to establish a relationship between local and global instability properties. In particular, does the existence of a region of local absolute instability imply that the entire flow can sustain temporally growing *global modes*?

It is appropriate at this point to briefly recall the classical hydrodynamic-instability description of open flows. Since several spatially developing shear flows are known to be extremely sensitive to external noise, many controlled experiments have been conducted to determine their response to different excitation frequencies. As a result, it has been customary to represent the downstream development of vortical structures as a collection of spatially growing instability waves of various frequencies [see Ho & Huerre (1984) for a review of such analyses applied to mixing layers]. In other words, experimental observations have, in general, been compared with the results of local spatial stability calculations (with given real frequency and unknown complex wave number) performed on the measured time-averaged mean velocity profile at each streamwise station. Such an approach has been reasonably successful in describing the evolution of vortices in forced experiments. For examples of this type of analysis, the reader is referred to Crighton & Gaster (1976) and Gaster et al. (1985), among many other similar studies. A large part of the hydrodynamic-stability literature, however, has been devoted to *temporal theory* (with given real wave number and unknown complex frequency), where it is implicitly assumed that the flow develops from some given initial state. The following question may then be asked: What is the fundamental reason for adopting a spatial theory point of view in many open shear flows? It is argued here that the notions of local absolute/convective instability provide a rigorous justification for selecting spatial theory in specific open flows (homogeneous mixing layers, flat-plate wakes, uniform-density jets). More interestingly, application of these concepts to other open flows (bluff-body wakes, heated jets) leads to the conclusion that local spatial theory

in the strict sense (real frequency) is not appropriate. Wave number and frequency both need to be considered complex, and a global temporal instability may arise whereby the entire nonparallel mean flow admits self-sustained global modes with well-defined complex frequencies.

Local/global and absolute/convective instability concepts provide the necessary theoretical framework to classify different open shear flows according to the qualitative nature of their dynamical behavior. For instance, shear flows that are locally convectively unstable everywhere (mixing layers, flat-plate wakes) essentially display extrinsic dynamics. The spatial evolution of the unsteady flow is in large part determined by the character (amplitude, frequency content, etc.) of the excitation that can be tailored to meet specific control goals. Such flows are *noise amplifiers*. By contrast, shear flows with a pocket of absolute instability of sufficiently large size (bluff-body wakes, hot or low-density jets) may display intrinsic dynamics of the same nature as in closed-flow systems. Fluid particles are still advected downstream, but temporally growing global modes may be present. These flows behave as *oscillators*: The evolution of vortices does not rely on the spatial amplification of external perturbations but rather on the growth of initial disturbances in time. Furthermore, the distribution of global modes is synchronized in the streamwise direction. This class of open flows is particularly well suited to a nonlinear dynamical-systems approach of the kind that has been implemented in closed systems. The onset of deterministic chaos, if it exists, is likely to be well defined in these systems: One expects a well-ordered sequence of bifurcations leading from a limit cycle (the global mode) to a low-dimensional strange attractor. The sensitivity of convectively unstable flows to external noise, on the other hand, makes it much more difficult to discriminate between low-dimensional chaos arising from the flow dynamics and spatially amplified random noise. Finally, there exists a third class of marginally globally stable flows (homogeneous jets) where the local velocity profiles are, strictly speaking, locally convectively unstable in the entire field but absolute instability is incipient at some streamwise station. In such situations, global modes are often weakly damped in time, and they can be preferentially destabilized by applying external forcing in the vicinity of the global-mode frequency.

The distinction between absolute and convective instabilities appears to have first been brought out in a general context by Twiss (1951a,b, 1952) and Landau & Lifshitz (1954, 1959). It should be emphasized that plasma physicists have made extensive and seminal contributions to the theoretical foundations underlying these notions, and that they have applied them to the study of numerous plasma instabilities. For systematic developments of the main ideas, the reader is referred to the work of Sturrock (1958,

1961), Briggs (1964), Akhiezer & Polovin (1971), Bers (1975, 1983), and Lifshitz & Pitaevskii (1981). The complete and lucid review of Bers (1983) is particularly recommended for an up-to-date account of recent theoretical efforts in the description of spatio-temporal plasma instabilities. The topic of absolute/convective instabilities has found its way into the mainstream of the plasma-physics literature: Presentations of the main ideas have appeared in the books by Clemmow & Dougherty (1969), Mikhailovskii (1974), and Cap (1976), among others.

The impact of such concepts on the study of fluid-mechanical instabilities appears to be of much more recent origin. A spatio-temporal description of Tollmien-Schlichting wave packets in boundary layers was developed early on by Gaster (1968, 1975), and a general formal methodology was proposed without explicitly introducing a definite distinction between the absolute or convective nature of the instability mechanism. The technique advocated by Briggs (1964) has been repeatedly implemented by Tam (1971, 1978, 1981) to analyze the receptivity of compressible shear flows to acoustic forcing. In geophysical fluid dynamics, Thacker (1976) and Merkine (1977) have determined the transition from absolute to convective instability in a two-layer model of the baroclinic instability. But, it is mostly in the last five years that these issues have come to the foreground in the description of hydrodynamic instabilities in spatially evolving shear flows. We wish to report here on these recent advances. Only a few survey articles have appeared that treat the subject from a fluid-mechanical point of view. One should mention, however, the reviews by Bechert (1985), Huerre (1987), and Monkewitz (1989b). Morkovin (1988) has recently proposed an appealing interpretation of roads to turbulence in open shear flows that primarily hinges on possible receptivity mechanisms and on the absolute/convective nature of instabilities in various shear flows.

The present review is organized in the following manner. Sections 2 and 3 are devoted to a formal presentation of local and global instability issues without being too specific about the particular flow under consideration. Absolute and convective instabilities are precisely defined for strictly parallel flows in Section 2, together with the mathematical criterion determining the nature of the instability. In Section 3 we define global instability and relate the local instability properties to the presence or absence of self-sustained global modes in spatially developing flows. In Sections 4, 5, and 6 we discuss how these general ideas have enhanced our qualitative and quantitative understanding of the dynamical behavior of specific shear flows. The approach in these three sections is far more descriptive. In Section 4 globally stable flows are discussed, whereas Sections 5 and 6

pertain to marginally globally stable flows and globally unstable flows, respectively. Instead of being exhaustive, we have chosen in the text to discuss only a few illustrative examples in each section. However, for the sake of comprehensiveness, the scope and results of relevant studies have been summarized (see Appendix) in a series of four tables pertaining to wall-bounded shear flows, single mixing layers, wakes, and jets, respectively. The final section is devoted to a number of related issues: experimental diagnostics, implications for flow control, chaotic dynamics in open flows, and finally pattern propagation fronts.

2. LOCAL INSTABILITY CONCEPTS: PARALLEL FLOWS

The classical linear stability theory of parallel shear flows is concerned with the development in space and time of infinitesimal perturbations around a given basic flow $U(y;R)$. In the sequel, x, y, and t denote the streamwise direction, cross-stream direction, and time, respectively, and $U(y;R)$ is the sole component of the basic flow in the x-direction. The basic state is parallel, i.e. it is assumed to be independent of x but may vary with a control parameter R, such as the Reynolds number. Fluctuations are typically decomposed into elementary instability waves $\phi(y;k)\exp\{i(kx-\omega t)\}$ of complex wave number k and complex frequency ω. The cross-stream distribution $\phi(y;k)$ is then shown in most cases to satisfy an ordinary differential equation of the Orr-Sommerfeld type. Enforcement of appropriate boundary conditions at, say, y_1 and y_2 then leads to an eigenvalue problem whereby eigenfunctions $\phi(y;k)$ exist only if k and ω are constrained to satisfy a dispersion relation of the form

$$D[k,\omega;R]=0. \tag{1}$$

For simple basic flows, this relation can be calculated explicitly. For more realistic velocity profiles, it is obtained by numerical integration of the Orr-Sommerfeld equation. *Temporal modes* $\omega(k;R)$ refer to cases where the complex frequency ω is determined as a function of real wave number k. Conversely, *spatial branches* $k(\omega;R)$ are obtained by solving for complex wave numbers k when ω is given real. In this section we deliberately ignore variations in the cross-stream direction y and only consider the spatio-temporal evolution of instability waves in the (x,t)-plane. This projection greatly simplifies the presentation of the fundamental concepts without losing any of the essential characteristics of the instability. Thus, one may associate a differential or integro-differential operator $D[-i(\partial/\partial x), i(\partial/\partial t);R]$ in physical space (x,t) to the dispersion relation (1) in spectral space (k,ω),

such that fluctuations $\psi(x, t)$ satisfy

$$D\left[-i\frac{\partial}{\partial x}, i\frac{\partial}{\partial t}; R\right]\psi(x, t) = 0. \tag{2}$$

The mathematical framework to be outlined next has proven to be extremely valuable in the study of plasma instabilities. For detailed discussions within this context, the reader is referred to Sturrock (1961), Briggs (1964), Bers (1975, 1983) and Lifshitz & Pitaevskii (1981). One of us (Huerre 1987) has recently reviewed this subject from the point of view of fluid-dynamical instabilities.

Following these earlier analyses, one introduces the Green's function, i.e. the impulse response $G(x, t)$ of the flow defined by

$$D\left[-i\frac{\partial}{\partial x}, i\frac{\partial}{\partial t}; R\right]G(x, t) = \delta(x)\delta(t), \tag{3}$$

with δ denoting the Dirac delta function.

The basic flow is then said to be linearly *stable* if

$$\lim_{t\to\infty} G(x, t) = 0 \text{ along all rays } x/t = \text{constant}, \tag{4}$$

and it is linearly *unstable* if

$$\lim_{t\to\infty} G(x, t) = \infty \text{ along at least one ray } x/t = \text{constant}. \tag{5}$$

Among linearly unstable flows, one must further distinguish between two types of impulse response: The basic flow is referred to as *convectively unstable* if

$$\lim_{t\to\infty} G(x, t) = 0 \text{ along the ray } x/t = 0, \tag{6}$$

and it is *absolutely unstable* if

$$\lim_{t\to\infty} G(x, t) = \infty \text{ along the ray } x/t = 0. \tag{7}$$

The above definitions can be illustrated on the linearized Ginzburg-Landau model. The operator D then takes the form

$$D\left[-i\frac{\partial}{\partial x}, i\frac{\partial}{\partial t}; R\right]\psi(x, t) \equiv \frac{\partial\psi}{\partial t} + \omega_k\frac{\partial\psi}{\partial x} - \frac{i}{2}\omega_{kk}\frac{\partial^2\psi}{\partial x^2} + i\omega_R(R - R_c)\psi = 0, \tag{8}$$

where ω_k is a real positive constant group velocity, and ω_{kk} and ω_R are complex constants with $\omega_{kk,i} < 0$. When an appropriate cubic nonlinearity

is added, this simple model is known to arise in many marginal-stability analyses of fluid-dynamical systems close to onset (Newell & Whitehead 1969, Stewartson & Stuart 1971). In such a context, the field $\psi(x, t)$ is interpreted as a complex amplitude function characterizing the spatio-temporal modulations of the marginal wave $\psi(x, t)e^{i(k_c x - \omega_c t)}$ at $R = R_c$. The Ginzburg-Landau equation has been extensively studied by Deissler (1985, 1987a,c, 1989) to identify possible transition mechanisms in open-flow systems (see Section 7). Throughout the present review, we use Equation (8) and its spectral counterpart as a simple example of instability-wave evolution. It is argued in the next section that the spatio-temporal dynamics of global modes is indeed governed, in the WKB approximation, by such an amplitude equation, but with varying coefficients.

Examples of possible linear impulse responses arising from Equation (8) are displayed in Figure 1 for different ranges of the control parameter R (see also Chomaz et al. 1987). Disturbances grow exponentially along all rays contained within the indicated wedges. The flow is stable in Figures 1*a,d,f*, convectively unstable in Figures 1*b,g*, and absolutely unstable in

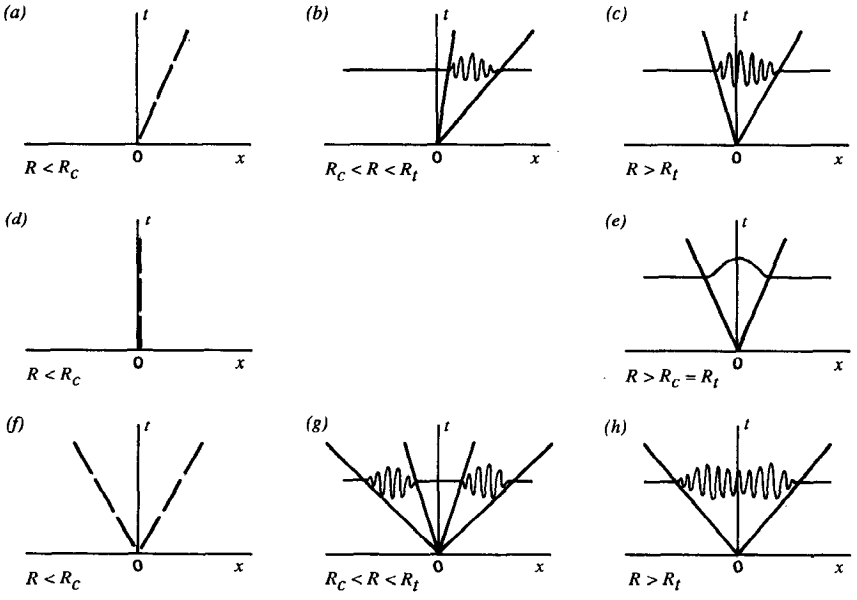

Figure 1 Sketches of typical impulse responses. Single traveling wave: (*a*) stable, (*b*) convectively unstable, (*c*) absolutely unstable. Stationary mode: (*d*) stable, (*e*) absolutely unstable. Counterpropagating traveling waves: (*f*) stable, (*g*) convectively unstable, (*h*) absolutely unstable.

Figures 1*c*,*e*,*h*. Typically, convectively unstable flows give rise to wave packets that move away from the source and ultimately leave the medium in its undisturbed state. Absolutely unstable flows, by contrast, are gradually contaminated everywhere by a point-source input.

Three scenarios, among others, can be envisioned as the control parameter R is varied. These can be visualized by following the sketches of Figure 1 along three horizontal levels. In the general case, where no particular spatial symmetries prevail, the critical value R_c marks the transition from a stable flow (Figure 1*a*) to a convectively unstable flow (Figure 1*b*). When cubic nonlinear terms are included, the system undergoes, at this same value R_c, a Hopf bifurcation to a limit cycle in the form of a *spatially periodic traveling wave*. There may also exist a second transition point $R_t > R_c$ beyond which the flow becomes absolutely unstable (Figure 1*c*). By contrast, in physical situations such as Rayleigh-Bénard convection or Taylor-Couette flow, an additional reflection symmetry $x \to -x$ is present and R_c necessarily coincides with R_t (Figures 1*d*,*e*). In Equation (8), ω_k is equal to zero, and ω_{kk}, ω_R are in this case purely imaginary. The flow then undergoes at R_c a stationary bifurcation to a steady state. In contrast with the general case, such flows are absolutely unstable immediately beyond the onset of instability. Finally, we note the scenario one may expect when there is a Hopf bifurcation to an *oscillatory spatially periodic state* in systems endowed with reflection symmetry $x \to -x$. Such a situation has recently been studied to describe oscillating convection in binary fluids (Coullet et al. 1985, Cross 1986, 1988, Deissler & Brand 1988). The instability can then be decomposed into left- and right-moving waves of respective complex amplitudes ψ_L and ψ_R; each family of waves is governed by a Ginzburg-Landau equation of the form (8) with opposite signs of the group velocity ω_k. Above the bifurcation point R_c, the instability is necessarily convective (Figure 1*g*) but there may be a critical value $R_t > R_c$ beyond which both wave packets merge to give rise to absolute instability (Figure 1*h*).

General mathematical criteria based on the properties of the dispersion relation D in the complex k- and ω-planes have been derived to determine the nature of the instability. Equation (3) can immediately be solved in (k, ω)-space. The Green's function is therefore expressed as the double Fourier integral

$$G(x,t) = \frac{1}{(2\pi)^2} \int_F \int_L \frac{e^{i(kx-\omega t)}}{D[k,\omega;R]} d\omega\, dk. \tag{9}$$

The contour L in the complex frequency plane is a straight horizontal line located above all the singularities of the integrand so as to satisfy causality,

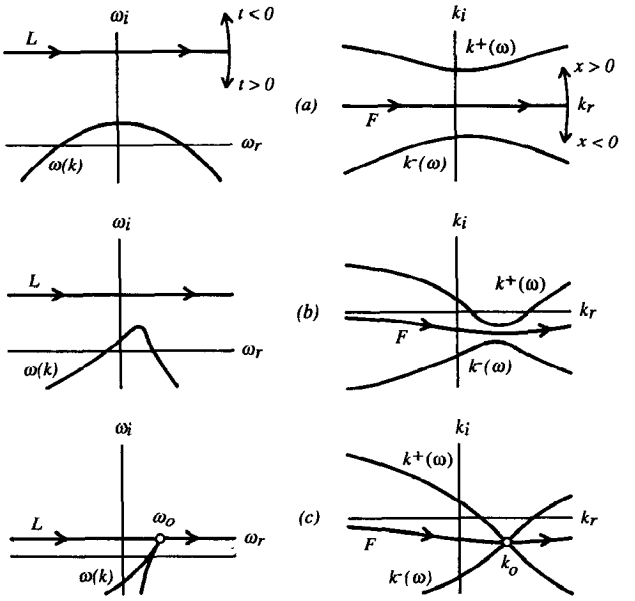

Figure 2 Loci of spatial branches $k^+(\omega)$ and $k^-(\omega)$ as L-contour is displaced downward in the complex ω-plane. (*a*), (*b*), and (*c*) refer to different stages of the pinching process.

namely $G(x, t) = 0$ for all x when $t < 0$. The path F in the complex wavenumber plane is initially taken along the real axis. A sketch of the paths of integration is shown in Figure 2*a*. If one assumes for simplicity that Equation (1) admits a single discrete temporal mode $\omega(k)$, then the Green's function $G(x, t)$ is formally obtained from a residue calculation in the ω-plane at $\omega = \omega(k)$. One finds that

$$G(x,t) = -\frac{i}{2\pi} H(t) \int_{-\infty}^{+\infty} \frac{e^{i[kx-\omega(k)t]}}{\dfrac{\partial D}{\partial \omega}[k, \omega(k); R]}\, dk, \tag{10}$$

where $H(t)$ is the Heaviside unit-step function. This Fourier integral over all wave numbers k can be evaluated for large time t (x/t fixed) by applying the method of steepest descent. Details of the calculation very much depend on the particular form of $\omega(k)$. It is assumed here that the mode $\omega(k)$ gives rise to a single stationary point k_* for the phase in the integrand such that

$$\frac{\partial \omega}{\partial k}(k_*) = \frac{x}{t}. \tag{11}$$

If the original contour of integration along the real k-axis can be deformed into a steepest descent path issuing from the saddle point k_*, $G(x, t)$ can be evaluated asymptotically for large time. Following standard arguments, one obtains

$$G(x,t) \sim -(2\pi)^{-1/2} e^{i\pi/4} \frac{e^{i[k_* x - \omega(k_*)t]}}{\dfrac{\partial D}{\partial \omega}[k_*, \omega(k_*)] \left[\dfrac{d^2\omega}{dk^2}(k_*)t\right]^{1/2}}. \tag{12}$$

The Green's function takes the form of a wave packet in the (x, t)-plane. Along each ray x/t within the packet, the response is dominated by a specific complex wave number k_* such that its real group velocity satisfies (11). The temporal growth rate along each ray reduces to $\sigma = \omega_i(k_*) - (x/t)k_{*i}$.

In most problems of interest, the temporal growth rate $\omega_i(k)$, k real, reaches a maximum $\omega_{i,\max} \equiv \omega_i(k_{\max})$ at a real value $k_{\max}$ such that

$$\frac{\partial \omega_i}{\partial k}(k_{\max}) = 0. \tag{13}$$

This same *maximum growth rate* $\omega_{i,\max}$ is observed within the wave packet $G(x, t)$ along the specific ray $x/t = \partial\omega_r/\partial k(k_{\max})$, and it is straightforward to show that it corresponds to the maximum attainable value of σ along any ray x/t. Based on definitions (4) and (5), one therefore arrives at the following trivial criterion for linear instability:

$$\begin{aligned} &\omega_{i,\max} > 0 \qquad \text{linearly unstable flow,} \\ &\omega_{i,\max} < 0 \qquad \text{linearly stable flow.} \end{aligned} \tag{14}$$

In order to distinguish between convective and absolute instabilities, it is further necessary to examine, according to definitions (6) and (7), the long-time behavior of the wave number k_0 observed along the ray $x/t = 0$ at a *fixed* spatial location. This complex k_0 has, by definition, a zero group velocity

$$\frac{\partial \omega}{\partial k}(k_0) = 0, \tag{15}$$

and the corresponding $\omega_0 \equiv \omega(k_0)$ is commonly called the *absolute frequency*. *The absolute growth rate* is then denoted by $\omega_{0,i} \equiv \omega_i(k_0)$. In other words, the absolute growth rate $\omega_{0,i}$ characterizes the temporal evolution of the wave number k_0 observed at a fixed station in the limit $t \to \infty$. By contrast, the maximum growth rate $\omega_{i,\max}$ defined previously is observed following the peak of the wave packet. Just as the sign of $\omega_{i,\max}$

determines the unstable/stable nature of the flow, the sign of $\omega_{0,i}$ determines its absolute/convective nature. One therefore is led to the following criterion:

$$\omega_{0,i} > 0 \qquad \text{absolutely unstable flow,}$$

$$\omega_{0,i} < 0 \qquad \text{convectively unstable flow.} \tag{16}$$

Typically, the absolute frequency ω_0 is an algebraic branch point of the function $k(\omega)$ in the complex ω-plane or, equivalently, k_0 is a saddle point of $\omega(k)$. It is important to note (Chomaz et al. 1989a) that the growth rate along any ray admits $\omega_{i,\max}$ as an upper bound, as mentioned previously. Thus, one necessarily has

$$\omega_{0,i} \leq \omega_{i,\max}. \tag{17}$$

Application of the above criterion to model equation (8) immediately leads to expressions for k_0 and ω_0. For future reference, one notes that the Ginzburg-Landau equation can then be recast in a form involving ω_{kk}, k_0, and ω_0 only:

$$\frac{\partial \psi}{\partial t} - \omega_{kk} k_0 \frac{\partial \psi}{\partial x} - \frac{i}{2}\omega_{kk} \frac{\partial^2 \psi}{\partial x^2} + i\left[\omega_0(R) + \frac{\omega_{kk}}{2} k_0^2\right]\psi = 0. \tag{18}$$

The dispersion relation associated with (18) is $\omega - \omega_0 = (\omega_{kk}/2)(k-k_0)^2$, a clear indication of the presence of a second-order algebraic branch point at $\omega = \omega_0$. The linearized Ginzburg-Landau equation is indeed the simplest evolution model giving rise to an absolute or convective instability.

As emphasized by Briggs (1964) and Bers (1975), the absolute/convective instability criterion given by Equations (15) and (16) is not precise enough as it stands. For the purpose of illustration, we assume that the temporal mode $\omega(k)$ exhibits a single second-order algebraic branch point ω_0 with only two spatial branches $k^+(\omega)$ and $k^-(\omega)$. One must then carefully monitor the loci of $k^+(\omega)$ and $k^-(\omega)$ when ω travels along the L contour. As a preliminary remark, it can be argued that when L is located above all the singularities of D, none of the spatial branches $k^+(\omega)$ and $k^-(\omega)$ can cross the horizontal line F in the complex k-plane (see, for instance, Figure 2*a*). When $x > 0$ ($x < 0$), the contour F is closed in the upper (lower) half k-plane and different spatial branches $k^+(\omega)$ and $k^-(\omega)$ contribute to the response in different regions of physical space. Two radically distinct situations may then take place.

First, as depicted in Figure 2*a*, the spatial branches k^+ and k^- may be located, when L is high enough, on opposite sides of F. Then, as L is displaced downward, both curves move toward each other (Figure 2*b*). In

this process, one must correspondingly deform the original contour F. Of course, the simultaneous deformation of L and F must cease when L touches $\omega(k)$ and F becomes "pinched" between the branches $k^+(\omega)$ and $k^-(\omega)$, as sketched in Figure 2*c*. Pinching occurs precisely at the point k_0 where the group velocity $\partial\omega/\partial k$ is zero. Correspondingly, a cusp appears at ω_0 in the locus of $\omega(k)$, a feature that can be used to detect the branch point, as demonstrated by Kupfer et al. (1987). If the corresponding ω_0 is located in the upper half ω-plane, the instability is absolute. Otherwise, it is convective. This method of determining whether an instability is absolute or convective is commonly called the Briggs (1964) criterion. In the Soviet literature (see, for instance, Mikhailovskii 1974) it is referred to as the Fainberg-Kurilko-Shapiro (1961) condition.

Other situations may also arise (Bers 1983, Pierrehumbert 1986, Huerre 1987, 1988) when the Riemann sheets of the branch point ω_0 correspond to spatial branches [say $k_1^+(\omega)$ and $k_1^+(\omega)$] located, for high enough L, in the same half k-plane. When the contour L is lowered, no pinching of F can occur and the corresponding branch point ω_0 is not the absolute growth rate. Thus, extreme care must be exercised to locate branch-point singularities pertaining to spatial branches $k^+(\omega)$ and $k^-(\omega)$ originating from distinct halves of the k-plane.

In the above discussion, we have only considered the simplest situation where $\omega(k)$ exhibits a saddle point at k_0. It should be observed, however, that the analytical structure of the dispersion relation needs to be studied in detail on a case-by-case basis in order to reach reliable conclusions regarding the nature of the instability. For instance, in flows such as mixing layers (Huerre 1983, Huerre & Monkewitz 1985), the temporal modes $\omega(k)$ display a nonanalytic behavior of the form $\omega \sim |k|$ as k approaches zero. A branch cut must then be introduced on the k_i axis to properly interpret the absolute value arising in the dispersion relation. Another approach, described in Huerre & Monkewitz (1985) and Huerre (1987), consists in associating with the real signal $\psi(x, t)$ the complex "*analytic signal*" $\Psi(x, t)$ defined by

$$\Psi(x,t) = \left[\delta(x) + \frac{i}{\pi x}\right] * \psi(x,t), \tag{19}$$

$$\psi(x,t) = \Psi_r(x,t). \tag{20}$$

The symbol $*$ denotes the convolution of two functions in x. The spectrum of $\Psi(x, t)$ is, by definition, restricted to positive wave numbers, and the study of the deformations of the spatial branches can be limited to the half-plane $k_r > 0$ and its corresponding image in the ω-plane. In this manner, $|k|$ can be replaced by k in the dispersion relation. The real signal

$\psi(x,t)$ is retrieved at the end of the calculations by taking the real part of $\Psi(x,t)$.

It may also happen that no branch points ω_0 where $\partial\omega/\partial k = 0$ can be found in the finite complex ω-plane. This peculiar behavior arises in the Görtler instability of the asymptotic profile on a concave plate (Park & Huerre 1988). The criterion (16) is not directly applicable, and one must resort to a direct numerical evaluation of $G(x,t)$ to safely conclude that this flow is indeed convectively unstable.

The physical significance of the spatial branches $k^+(\omega)$ and $k^-(\omega)$ becomes evident when one considers the response of a system to a monochromatic excitation of frequency ω_f applied at, say, $x = 0$ and switched on at $t = 0$. The field $\psi(x,t)$ is such that

$$D\left[-i\frac{\partial}{\partial x}, i\frac{\partial}{\partial t}; R\right]\psi(x,t) = \delta(x)H(t)e^{-i\omega_f t}. \tag{21}$$

A solution of this problem is readily obtained in Fourier space. As in the case of $G(x,t)$, the inverse Fourier transform with respect to ω is evaluated from a residue calculation. If a single discrete temporal mode $\omega(k)$ exists, $\psi(x,t)$ takes the form of a Fourier integral over all wave numbers, namely

$$\psi(x,t) = \frac{1}{2\pi}\int_{-\infty}^{+\infty} \frac{e^{i[kx-\omega(k)t]}}{[\omega(k)-\omega_f]\dfrac{\partial D}{\partial\omega}[k,\omega(k);R]}\,dk + \frac{e^{-i\omega_f t}}{2\pi}\int_{-\infty}^{+\infty}\frac{e^{ikx}}{D[k,\omega_f;R]}\,dk. \tag{22}$$

As $t\to\infty$, the first term can be obtained asymptotically in exactly the same manner as before by applying the method of steepest descent. The second term is calculated by closing the contour F in the upper (lower) half k-plane for $x > 0$ ($x < 0$), as indicated in Figure 2*a*. Residue contributions arise from the $k^+(\omega_f)$ and $k^-(\omega_f)$ of the dispersion relation at the fixed frequency ω_f. One arrives at the following estimate:

$$\psi(x,t) \sim (2/\pi)^{1/2}e^{-i\pi/4}\frac{e^{i[k_*x-\omega(k_*)t]}}{[\omega(k_*)-\omega_f]\dfrac{\partial D}{\partial\omega}[k_*,\omega(k_*)]\left[\dfrac{d^2\omega}{dk^2}(k_*)t\right]^{1/2}} + i\frac{e^{i[k^+(\omega_f)x-\omega_f t]}}{\dfrac{\partial D}{\partial k}[k^+(\omega_f),\omega_f;R]}H(x) - i\frac{e^{i[k^-(\omega_f)x-\omega_f t]}}{\dfrac{\partial D}{\partial k}[k^-(\omega_f),\omega_f;R]}H(-x), \tag{23}$$

where k_* is given along the ray x/t by Equation (11), and $H(x)$ denotes the Heaviside unit step function. The response is composed of a switch-on transient of the same qualitative nature as the Green's function (12) and a "steady-state" response arising from forcing the flow at the frequency ω_f. Spatially growing and/or decaying waves are located on either side of the source at $x = 0$. It is important to note that the spatial branches $k^+(\omega_f)$ and $k^-(\omega_f)$ have unambiguously been assigned to the domains $x > 0$ and $x < 0$, respectively. This can only be achieved if one has a priori determined (see Figure 2) that, for high enough L, they originate from the upper and lower half k-plane, respectively. If the flow is absolutely unstable, the transient part of the solution will, by definition, contaminate the "steady-state" response at all stations x, thereby making the signaling problem meaningless. If the flow is convectively unstable, transients move away from the source and one observes the steady-state signal associated with the spatial waves. It can be concluded that spatially growing waves at a real frequency ω_f are only of interest in convectively unstable flows. This feature becomes particularly obvious in Section 4, where we discuss examples of convectively unstable shear flows.

The characteristics of the spatial branches are sketched in Figure 3 in the case of the linearized Ginzburg-Landau equation. The solid curves pertain to a value of R in the convectively unstable range $R_c < R < R_t$, where k^+ and k^- are well separated (see also Figure 2*a*). When R exceeds R_t and the flow becomes absolutely unstable, the branches switch, as illustrated by the dashed curves. Thus, as R increases through R_t, the frequency ω_0 crosses the real ω-axis, and the corresponding saddle point k_0 leads to splitting of the branches in its vicinity. Branch switching in spatial stability calculations can be effectively used as an indication of a qualitative change in the nature of the instability from convective to absolute.

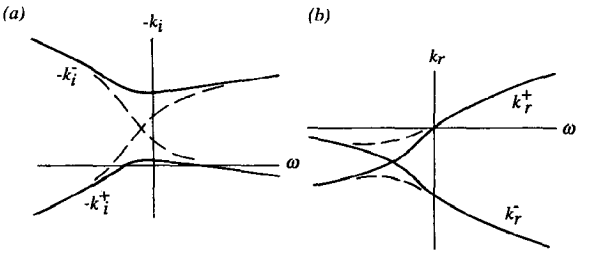

Figure 3 Spatial branches k^+ and k^- of the Ginzburg-Landau equation in the convectively unstable case (——). (*a*) spatial growth rate $-k_i$ versus real frequency ω; (*b*) k_r versus ω. Branch interchange in the absolutely unstable case (- - - -).

The concepts introduced in this section may very well appear to be trivial: A flow that is convectively unstable in one reference frame becomes absolutely unstable in another. There is no preferred laboratory frame in parallel flows that are invariant under Galilean transformations. We therefore wish to emphasize that absolute/convective instability properties become relevant precisely when Galilean invariance is broken. This is achieved either by applying an external perturbation at a fixed downstream station as described above, or by imposing no-slip conditions at the walls as in plane Poiseuille flow, or finally by allowing the flow to develop spatially. In all such cases, a unique laboratory frame is selected and local instability characteristics are unambiguously defined. In the next section, we examine one particular example of broken Galilean invariance, namely spatially developing flows.

3. GLOBAL-INSTABILITY CONCEPTS: SPATIALLY EVOLVING FLOWS

The previous section dealt with absolute/convective instability concepts in strictly parallel flows, i.e. basic flows that are invariant under continuous translations in the streamwise x-direction. Most shear flows of interest, however, such as mixing layers, jets, wakes, and boundary layers, are nonuniform in x. The purpose of the present section is to emphasize the deep relationship that exists between, on the one hand, the local instability characteristics at each streamwise x-station and, on the other hand, the global instability properties over many wavelengths of the instability.

The spatial development of the basic flow is typically characterized by an evolution length scale L defined as

$$\frac{1}{L} \simeq \frac{1}{\theta}\frac{d\theta}{dx}, \tag{24}$$

where $\theta(x)$ is, say, the local momentum or vorticity thickness. The main parameter of interest is then the ratio

$$\varepsilon \sim \frac{\lambda}{L} \ll 1, \tag{25}$$

where λ is a typical instability wavelength. If the streamwise coordinate x is nondimensionalized with respect to λ, the basic flow changes over a slow space scale $X = \varepsilon x$ and takes the form $U[y; \theta(X)]$, where $\theta(X)$ is in effect a local control parameter. One of the crucial hypotheses here is that ε is small. A breakdown of this assumption would preclude any possible connection between local and global instability properties. Following the

general framework previously outlined, fluctuations $\psi(x, t)$ now satisfy a linear partial differential operator of the form

$$L\left[-i\frac{\partial}{\partial x}, i\frac{\partial}{\partial t}; \theta(X), \varepsilon\frac{d\theta}{dX}, \ldots; R\right]\psi = 0. \tag{26}$$

The local dispersion relation is recovered by freezing X, so that

$$D[k, \omega; X, R] \equiv L[k, \omega; \theta(X), 0, \ldots; R]. \tag{27}$$

Absolute/convective instability concepts are readily applicable to (27). In particular, if the dispersion relation admits a single mode of the form $\omega[k; X; R]$, one defines a *local absolute frequency* $\omega_0(X; R)$ and its corresponding wave number $k_0(X; R)$, given by

$$\frac{\partial\omega}{\partial k}(k_0; X; R) = 0, \qquad \omega_0(X; R) \equiv \omega(k_0; X; R). \tag{28}$$

Similarly, one introduces a local complex frequency $\omega_{\max}(X; R)$, a local maximum growth rate $\omega_{i,\max}(X; R)$, and corresponding wave number $k_{\max}(X; R)$, such that

$$\frac{\partial\omega_i}{\partial k}(k_{\max}; X; R) = 0, \qquad \omega_{\max}(X; R) \equiv \omega(k_{\max}; X; R). \tag{29}$$

The Ginzburg-Landau evolution model can then be generalized by allowing k_0 and ω_0 appearing in (18) to depend on X. As is justified later, we choose to keep the leading-order terms in a Taylor expansion of k_0 and ω_0 around a point X_s in the complex X-plane such that $\partial\omega_0/\partial X = 0$. Thus, one assumes that

$$\omega_0(X; R) = \omega_s(R) + \frac{\omega_{0XX}}{2}(X - X_s)^2, \tag{30}$$

$$k_0(X; R) = k_0(X) = k_s + k_{0X}(X - X_s), \tag{31}$$

where k_s, k_{0X}, and ω_{0XX} are given complex constants with $\omega_{0XX,i} < 0$, and $\omega_{s,i}(R)$ is a monotonically increasing function of R.

Spatially developing flows may then be divided into four broad classes according to the nature of the local instability at each streamwise station. Typical configurations have been illustrated in Figures 4*a–d*. In the first class (Figure 4*a*), the flow is *locally stable uniformly* along the streamwise direction and $\omega_{i,\max} < 0$, $\omega_{0,i} < 0$ for all X. When a region of local convective instability is present (Figure 4*b*) where $\omega_{i,\max} > 0$, $\omega_{0,i} < 0$, the flow is said to be *locally convectively unstable*. Such systems behave as amplifiers of external disturbances. They are *globally stable* in the sense that no self-sustained resonant states may arise. The term "globally stable" is used

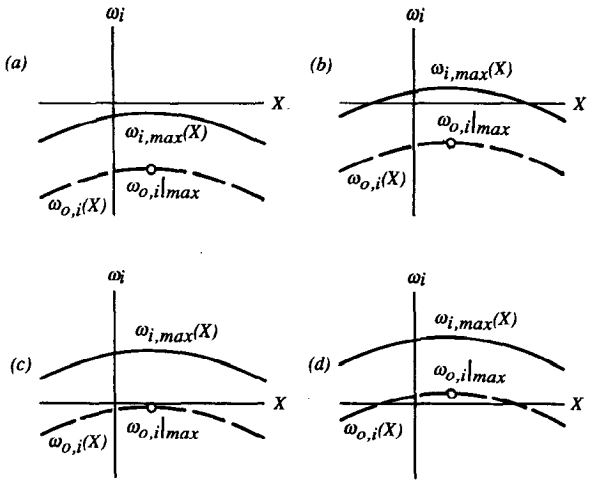

Figure 4 Classes of spatially developing flows according to the nature of the local instability. (*a*) uniformly stable; (*b*) convectively unstable; (*c*) almost absolutely unstable; (*d*) pocket of absolute instability.

here with a meaning that is different from classical hydrodynamic stability theory. We do not imply that the flow is stable to all finite-amplitude perturbations, merely that it is stable with respect to global infinitesimal fluctuations in the entire flow field. Specific examples are discussed in Section 4. In the third class of flows, the maximum absolute growth rate over all X, $\omega_{0,i}|_{\max}$, is still negative but very small (Figure 4*c*). As mentioned in Section 5, these *almost absolutely unstable flows* may admit weakly damped global modes that are preferentially amplified by forcing the flow in the neighborhood of the global frequency. They are *marginally globally stable*. Finally, in the fourth class of flows (Figure 4*d*), the curve $\omega_{0,i}(X; R)$ has crossed the X-axis and *local absolute instability* prevails in a finite region along the stream. It is argued later in this section that such systems may exhibit self-excited *global modes* at specific complex frequencies ω_G: They are *globally unstable*. Examples of locally absolutely unstable flows are presented in Section 6. It should be emphasized that some shear flows may change from one class to another as the control parameter R is varied, whereas others remain within the same class.

3.1 *Signaling Problem in Locally Convectively Unstable Flows*

Most linear stability analyses of spatially developing flows have been restricted to locally convectively unstable situations of the kind illustrated

in Figure 4*b*. For instance, the WKB approximation has been applied to circular jets by Crighton & Gaster (1976) and to mixing layers by Gaster et al. (1985). There is an extensive literature on the subject, and one only needs to recall here the salient features of this type of analysis. The starting point is the governing linear partial differential equation (26). It is assumed that, at $x = X = 0$, the flow is excited at a given real frequency ω_f, and a time-periodic response is sought in the form

$$\psi(x, t; X) = \phi^{\pm}(x; X)e^{-i\omega_f t}, \tag{32}$$

where the + and − superscripts pertain to the domains $x > 0$ and $x < 0$ on either side of the source. Since the flow is slowly evolving on the streamwise scale $X = \varepsilon x$, it is legitimate to seek leading-order approximations

$$\phi^{\pm}(x; X) \sim A^{\pm}(X) \exp\left[\frac{i}{\varepsilon}\int k^{\pm}(X; \omega_f)\, dX\right], \tag{33}$$

where the spatial branches k^+ and k^- satisfy the local dispersion relation

$$D[k^{\pm}(X; \omega_f), \omega_f; X; R] = 0. \tag{34}$$

We note that the downstream and upstream branches k^+ and k^- are unambiguously identified by following, for each X, the contour-deformation arguments outlined in Section 2 (see Figure 2). Application of a standard multiple-scale formalism to the governing equation (26) then leads at $O(\varepsilon)$ to the linear evolution equations for the complex amplitudes A^+ and A^-:

$$i\frac{\partial \omega}{\partial k}[k^{\pm}(X; \omega_f)]\frac{dA^{\pm}}{dX} + p^{\pm}(X)A^{\pm} = 0, \tag{35}$$

where $p^{\pm}(X)$ are computed by imposing suitable orthogonality conditions.

The WKB solution (33) is seen to capture the global response of the flow over streamwise distances of the order of L, the evolution length scale of the basic state. This method allows a comprehensive treatment of the receptivity of a given flow to various input frequencies. In particular, one may determine the specific forcing frequency ω_f that will achieve the maximum amplitude gain over the total streamwise extent of the flow. Results of this formulation are illustrated in Figure 5. Within the unstable frequency band, one obtains amplified waves in the region $x > 0$ and a decaying tail upstream of the source ($x < 0$).

3.2 *Global Modes in Spatially Developing Flows*

In the previous analysis, we examined the response to a perturbation of known *real* frequency ω_f. However, spatially developing flows might very

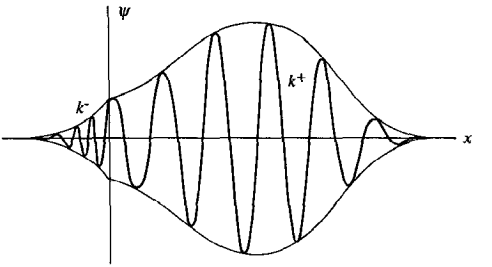

Figure 5 Sketch of response to time-harmonic forcing in spatially developing flows.

well support self-excited global modes in the absence of external forcing. In the present context, a global-mode solution is defined as

$$\psi(x,t;X) = \phi(x;X)e^{-i\omega_G t}. \tag{36}$$

In contrast with the signaling problem, the complex frequency ω_G is an unknown quantity. Its value is to be determined by solving the governing equation (26) for $\phi(x;X)$, subject to suitable homogeneous boundary conditions. For the class of doubly infinite systems under consideration here (see Figure 4), it is required that disturbances decay at $x = \pm\infty$. On a semiinfinite domain $0 < x < \infty$, one could impose, for instance, the condition that ψ be zero at $x = 0, \infty$. In any case, the complex frequency ω_G is now an eigenvalue and $\phi(x;X)$ its associated streamwise eigenfunction. The obvious *criterion for global stability or instability* is

$$\begin{aligned} &\omega_{G,i} < 0 \qquad \text{globally stable flow,} \\ &\omega_{G,i} > 0 \qquad \text{globally unstable flow.} \end{aligned} \tag{37}$$

Several global modes are in general possible, and in order to ensure stability, one naturally must require that $\omega_{G,i}$ be negative for all eigenvalues. The limiting case $\omega_{G,i} = 0$ marks in general a bifurcation point to a global mode for the entire flow. An example of a global-mode solution is shown in Figure 6 for the Ginzburg-Landau model (18) with varying coefficients (30)–(31) on a doubly infinite domain. The smooth shape of ϕ should be compared with the discontinuous solution of the response problem sketched in Figure 5. More importantly, note that at the location where the local absolute growth rate $\omega_{0,i}$ reaches a maximum, the global-mode amplitude is still very small compared with its maximum. This situation does not seem to be exceptional and serves to dispel the notion that the region of local absolute instability, and in particular the region where $\omega_{0,i}$ is largest, coincides with the region in which the "action" is observed (i.e. where global modes reach maximum amplitude). Hence, a

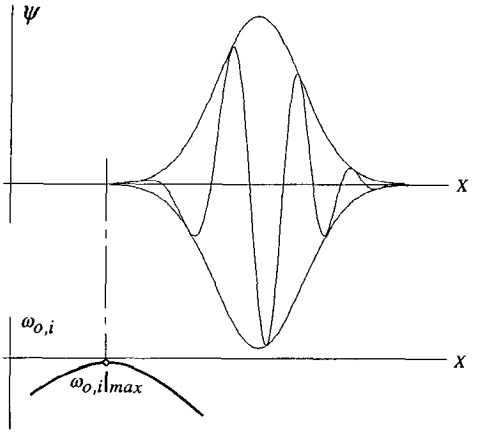

Figure 6 Global mode in spatially developing flows according to the Ginzburg-Landau model with the underlying absolute growth rate $\omega_{0,i}(x)$.

picture of a rather subtle, self-excited, low-amplitude "wavemaker" in the region of local absolute instability emerges, which acts as a source for the downstream instability wave(s). These latter waves develop downstream in a fashion very similar to ordinary spatial modes and reach a maximum amplitude approximately where they become neutral on a locally parallel basis.

It is natural to inquire whether the existence and the characteristics of global modes are at all related to the local instability properties of a given flow, as sketched in Figure 4. The possibility of a self-excited resonance due to the presence of a region of local absolute instability was first explored by Pierrehumbert (1984) for a zonally varying two-layer model of the baroclinic instability. The configuration was essentially the same as in Figure 4*d*. It was demonstrated that the slowly varying baroclinic flow in a doubly infinite domain could support global modes growing at the maximum absolute growth rate $\omega_{0,i}|_{\max}$ over the entire streamwise extent of the flow ($-\infty < x < +\infty$). Koch (1985) considered instead the semi-infinite spatially developing mean flow in the wake of bluff bodies (see Section 6) and showed that a region of local absolute instability existed immediately behind the cylinder in the von Kármán vortex-street regime. The connection between local and global properties has been explored further by Chomaz et al. (1987, 1988) for the Ginzburg-Landau model on a semiinfinite domain $0 < x < \infty$ with boundary conditions $\psi(0) = \psi(\infty) = 0$. A stabilizing cubic nonlinearity was added to model (18), and the local absolute frequency was assumed to vary linearly as $\omega_0(X) = \omega_0(0) + \omega_0' X$, $\omega_{0,i}' < 0$. All other coefficients of the equations were

kept constant. The following scenario emerged as $\omega_{0,i}(0)$ was gradually increased. In the range of uniform local stability, the system exhibited global stability. As a region of local convective instability appeared near the origin $X = 0$, numerical simulations revealed a regime of global transient instability (Davis 1976) in the sense that disturbances grew in a finite region of the (x, t)-plane but the system remained globally stable for large time with no self-sustained resonances. With further increases in $\omega_{0,i}(0)$, a zone of local absolute instability occurred near $X = 0$. If that pocket was sufficiently small, the global transient instability persisted. Beyond a critical size, however, the system became globally unstable and a Hopf bifurcation to a self-sustained global mode took place. Thus, in the context of the simple model, it was concluded that the existence of a region of local absolute instability was a necessary but not sufficient condition for the existence of an amplified global mode. Similar conclusions were reached in numerical simulations of the Ginzburg-Landau model on a doubly infinite domain (Chomaz et al. 1989b), with parabolic variations of the local absolute frequency as in Equation (30). In Section 6 it is seen that the above scenario is entirely consistent with hydrodynamic-stability analyses and experimental observations in wakes and jets.

A fundamental question arises in the study of global-mode properties: What is the frequency-selection criterion for ω_G? More specifically, is it possible within the slowly varying WKB approximation to obtain a leading-order estimate of the global-mode frequency from local stability characteristics alone? As alluded to earlier, Pierrehumbert (1984) has suggested that in doubly infinite systems of the kind sketched in Figure 4, ω_G is given by $\omega_{0,r}|_{\max}$, namely the real part of ω_0 at the streamwise location of maximum absolute growth rate $\omega_{0,i}|_{\max}$. In semiinfinite systems $(0 < X < \infty)$ with a single pocket of absolute instability close to the origin, Koch (1985) proposes yet another selection principle: The global-mode frequency should, in his view, lock to the local absolute frequency $\omega_{0,r}(X_t) \equiv \omega_0(X_t)$ at the streamwise station X_t separating the absolute and convectively unstable regions. The authors of this review doubt that any of the above criteria could be rigorously justified from a theoretical point of view. It seems to us that in doubly infinite systems with local instability properties such as those described qualitatively in Figure 4 (i.e. a local absolute growth-rate curve with a single maximum), a more appropriate selection criterion is as follows: To leading order in the WKB parameter ε, the most unstable global-mode frequency is given by the local absolute frequency $\omega_s = \omega_0(X_s)$ at the point X_s in the complex X-plane such that

$$\frac{\partial \omega_0}{\partial X}(X_s) = 0. \tag{38}$$

The point X_s is the saddle point of the function $\omega_0(X)$ in the complex X-plane that lies closest to the real X-axis, as sketched in Figure 7. This result has been derived by Huerre et al. (1988) and Chomaz et al. (1989a) for a class of linear partial differential equations of the Ginzburg-Landau type (18) with arbitrary variations for $\omega_0(X)$ and $k_0(X)$. One of the essential assumptions of the study is that the function $\omega_0(X)$ exhibits a saddle point X_s in the complex X-plane. Furthermore, under these conditions, it is possible to show that the following inequalities hold:

$$\omega_{G,i} \leq \omega_{0,i}(X_s) \leq \omega_{0,i}|_{\max}, \tag{39}$$

where $\omega_{G,i}$ is the growth rate of any global mode, and $\omega_{0,i}|_{\max}$ is the maximum absolute growth rate over the real axis $-\infty < X < +\infty$. As a consequence of (39), we recover the fact that the existence of an amplified global mode with $\omega_{G,i} > 0$ necessarily implies a finite region of absolute instability—in other words, $\omega_{0,i}|_{\max} > 0$. The frequency-selection criterion (38) had in fact been implicitly derived by Bar-Sever & Merkine (1988) in the specific context of weakly diverging large-scale geophysical flows. A related "mode-conversion" formulation has been developed by Fuchs et al. (1981) to describe the evolution of instability waves in a weakly inhomogeneous plasma.

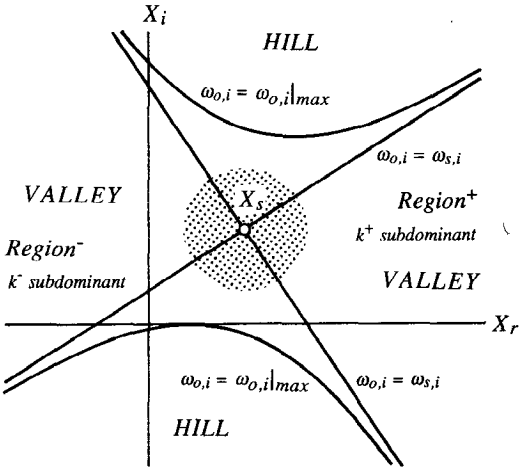

Figure 7 Sketch of different regions in the complex X-plane ($X = \varepsilon x$). The curves represent contours $\omega_{0,i}(X) =$ constant in the vicinity of the saddle point X_s. Shaded area denotes the inner turning-point region of size $O(\varepsilon^{1/2})$.

Going back to the original dispersion relation $\omega(k; X; R)$, the frequency-selection criterion takes the following symmetric form:

$$\frac{\partial \omega}{\partial k}(k_s; X_s; R) = 0, \qquad \frac{\partial \omega}{\partial X}(k_s; X_s; R) = 0, \qquad \omega_s = \omega(k_s; X_s; R). \tag{40}$$

It is interesting to see that the wave number k and streamwise coordinate X play the same role in (40). Both have to be considered complex, and the global-mode frequency ω_G is determined by the singularities of the local dispersion relation.

If a saddle point X_s of $\omega_0(X)$ exists in the complex X-plane, it is possible to develop a general formulation of global-mode characteristics from the linearized two-dimensional vorticity equation. Both the x- and y-coordinates are then eigenfunction directions, as discussed in Monkewitz et al. (1989b), and the theory is applicable to arbitrary spatially developing flows. Following the spirit of this review, we choose instead to outline the main features of the analysis, starting from the linear partial differential equation (26). The contours of constant $\omega_{0,i}(X)$ are assumed to be as in Figure 7, with a single maximum $\omega_{0,i}|_{max}$ of $\omega_{0,i}$ on the real X-axis, and global modes of the form (36) are sought with boundary conditions $\phi(\pm\infty; \pm\infty) = 0$. The unknown complex frequency ω_G is expanded as

$$\omega_G \sim \omega_s + \varepsilon\omega_2 + \ldots, \tag{41}$$

where ω_s is given by (38), and ω_2 is an unknown correction term. The methodology is similar to the one used by Pokrovskii & Khalatnikov (1961) in the study of particle reflection across a potential barrier. Several domains in the complex X-plane need to be considered separately. In the outer regions + and − (see Figure 7), the distribution of perturbations is expressed as in the signaling problem, namely

$$\phi^{\pm}(x; X) \sim A^{\pm}(X) \exp\left[\frac{i}{\varepsilon}\int_{X_s}^{X} k^{\pm}(X; \omega_s)\, dX\right]. \tag{42}$$

The branches k^+ and k^- are selected in the + and − regions, respectively, so as to satisfy the boundary conditions at $\pm\infty$. From the enforcement of orthogonality conditions at higher order, one is led to the evolution equations,

$$i\frac{\partial \omega}{\partial k}[k^{\pm}(X; \omega_s)]\frac{dA^{\pm}}{dX} + [\omega_2 + p^{\pm}(X)]A^{\pm} = 0, \tag{43}$$

which can be compared with the corresponding result (35) in the signaling problem.

In the turning-point region of size $O(\varepsilon^{1/2})$ around X_s (see Figure 7), an inner variable $\bar{X} = (X - X_s)/\varepsilon^{1/2}$ is introduced and the solution is given by

$$\bar{\phi}(x; X) \sim \mu(\varepsilon)\bar{A}(\bar{X})e^{ik_s(x-x_s)}, \tag{44}$$

where the gauge function $\mu(\varepsilon)$ and the amplitude function $\bar{A}(\bar{X})$ are unknown. The evolution equation for $\bar{A}(\bar{X})$ is determined, as before, by a suitable orthogonality condition applied at higher order. One finds

$$\frac{1}{2}\omega_{kk}\frac{d^2\bar{A}}{d\bar{X}^2} - i\omega_{kk}k_{0X}\bar{X}\frac{d\bar{A}}{d\bar{X}} + \left[\omega_2 - \delta\omega - \frac{1}{2}(\omega_{kk}k_{0X}^2 + \omega_{0XX})\bar{X}^2\right]\bar{A} = 0, \tag{45}$$

where the coefficients ω_{kk}, k_{0X}, and ω_{0XX} arise from the Taylor expansion of the dispersion relation $\omega(k; X)$ and of the absolute frequency $\omega_0(X)$ around k_s and X_s. The constant $\delta\omega$ is a genuinely nonlocal effect that need not concern us here. Provided one makes the substitution $-i\omega_2 \to \partial/\partial T$, the governing equation (45) in the inner region is seen to be of the linearized Ginzburg-Landau type (18). This is an a posteriori justification for choosing this model in the first place: It arises in a rational approximation scheme of global-mode characteristics in arbitrary spatially developing flows with local instability properties as sketched in Figure 7. The correction term ω_2 is determined by matching inner and outer solutions. A smooth "conversion" from the k^+ to the k^- branch occurs in the inner region provided that the global-mode frequency is restricted to take the discrete values

$$\omega_{Gn} \sim \omega_s + \varepsilon\left[\delta\omega - \frac{i}{2}\omega_{kk}k_{0X} + (\omega_{0XX}\omega_{kk})^{1/2}\left(n + \frac{1}{2}\right)\right], \tag{46}$$

where n is an integer. With the exception of the constant $\delta\omega$, the complex frequencies ω_{Gn} are solely expressed in terms of the local instability characteristics in the vicinity of the saddle point X_s.

The estimate (46) also holds when the y-structure is included (Monkewitz et al. 1989b). The eigenfunction distribution in y is then merely slaved to the slow variable X. Several caveats are in order, however. Formula (46) is only the result of a linearized analysis. It excludes nonlinear effects, which are likely to become important far away from bifurcation points. Furthermore, at large values of n the double turning point X_s is replaced by two first-order turning points X_{s1} and X_{s2}, and formula (46) becomes useless. The global eigenvalues ω_{Gn} are then determined by integral properties of the local dispersion relation over streamwise distance X.

It is convenient to think of Figure 7 as a level-contour plot of the surface $\omega_{0,i}(X_r, X_i)$, where the value of $\omega_{0,i}$ measures the "altitude," or level, of a

given point X. Since $\omega_{0,i}(X_s) \leq \omega_{0,i}|_{max}$, the point of maximum absolute growth rate on the real axis X_r is always on a "hill" of the saddle point X_s. We may then propose the following general scenario as a global control parameter R is increased. When $\omega_{0,i}|_{max}$ is negative, the flow is locally convectively unstable everywhere on the X_r-axis and the saddle point X_s is necessarily at a level $\omega_{0,i}(X_s) < 0$. According to the frequency-selection criterion, the flow is therefore globally stable. When $\omega_{0,i}|_{max}$ becomes positive, a pocket of absolute instability appears on the X_r-axis but the saddle point X_s may still be at a negative level, so that the flow remains globally stable. Finally, when the pocket of absolute instability reaches a critical finite size, the saddle point is raised to a level $\omega_{0,i}(X_s) > 0$ and a bifurcation to a self-sustained global mode takes place. If $B(t)$ denotes the complex amplitude of the global mode, the evolution equation near the global bifurcation point R_{G_c} is of the classical Landau form, namely

$$\frac{dB}{dt} = c_1(R - R_{G_c})B - c_2|B|^2B + \beta, \tag{47}$$

where $c_1(R - R_{G_c})$ is the linear temporal growth rate, and $c_{2r} > 0$ for a supercritical bifurcation. The complex constant β is a forcing term added for later reference.

4. EXAMPLES OF GLOBALLY STABLE FLOWS

In many cases where a purely convectively unstable open system is involved, some form of steady-periodic forcing is present, such as free-stream disturbances coupling into instability waves at solid trailing edges or other spatial inhomogeneities. As discussed above, in such systems the downstream evolution of linear disturbances in the long-time limit is described by spatial theory, pioneered by Gaster (1965), Michalke (1965), Tam (1971), and others. Any spatial development of the basic flow is thereby handled by locally parallel theory or, at a higher level, by the "slowly diverging" formulation (see Section 3.1 and, for instance, Crighton & Gaster 1976). A full discussion of the vast literature on fully convectively unstable flows is beyond the scope of this review, and only a few examples, which have explicitly been proven to be convectively unstable, are compiled in the summary tables. In an even smaller number of cases, such as the laminar flat-plate boundary layer (Gaster 1968, 1975, Gaster & Grant 1975), the rotating disk (Wilkinson & Malik 1985, Mack 1985, Reed & Saric 1989), and the mixing layer (Balsa 1988, 1989), the transient response has been investigated and found to correspond to the convective type sketched in Figure 1*b*.

The main point we want to make in this section is that global instability can arise from feedback not only by upstream-propagating vorticity (instability) waves, but also by irrotational global pressure feedback, governed in the incompressible inviscid limit by the Poisson equation

$$\nabla^2 p = \frac{\partial^2 (u_i u_j)}{\partial x_i \partial x_j}, \tag{48}$$

where p, u_i, and x_i denote the pressure, the three velocity components, and the usual Cartesian coordinates, respectively. As discussed by Ho & Huerre (1984, Sect. 5), Morkovin (1988), and Buell & Huerre (1988), the potentially most powerful sources in (48) are found on the boundaries of the flow domain or on solid boundaries within, although "volume sources" such as "vortex pairing" events in the mixing layer may also be significant (Dimotakis & Brown 1976, Laufer & Monkewitz 1980). It is well known that pressure feedback from solid surfaces placed into a shear flow downstream of its origin often leads to global instability in the form of "edge-," "collar-," "cavity-," and other tones (Rockwell & Naudascher 1979). Not surprisingly, the same effect can also be achieved "artificially" by electronic feedback, which is addressed in the conclusion.

More surprisingly, a global instability may also arise in numerical calculations carried out in finite computational "boxes." It was first noticed in a spatial mixing-layer calculation by Lowery & Reynolds (1986) that, depending on the length of the box, disturbances persisted indefinitely after the forcing was turned off. Buell & Huerre (1988) fully investigated this phenomenon and discovered that even without any intentional forcing, a transient is generated at the upstream boundary of the computational domain by the mismatch between the assumed initial condition at $t = 0$ and the boundary condition at $t > 0$, a mismatch that can only be avoided if the solution is known a priori. Figure 8 shows how the resulting wave packet propagates to the end of the box. There it creates a sharp pressure change that is instantaneously felt at the inflow boundary, generates a second wave packet, etc., until the multiple reflections lead to a self-sustained dynamical state, which is noisy for this particular box length. Such behavior demonstrates that numerical simulations, very much like laboratory experiments, may exhibit undesirable resonances and, generally speaking, be plagued by "facility effects."

A second point we wish to emphasize is that although the basic flow may be convectively unstable, instantaneous velocity profiles of the disturbed basic flow can be absolutely unstable with respect to secondary disturbances. Such a concept can be justified, if the scale of the secondary instability is very much smaller than the scale of the primary disturbance, and was first proposed by Landahl (1972) with specific reference to the

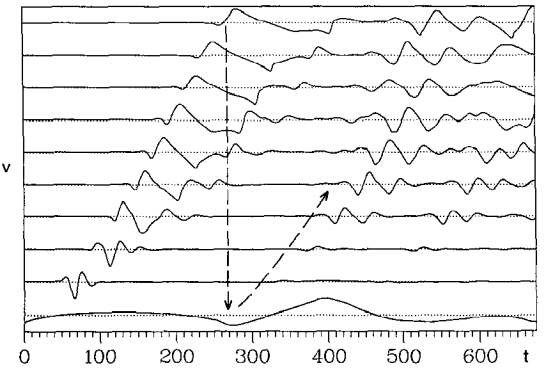

Figure 8 Time traces of velocity v at $x = 1, 50, 85, 115, 140, 160, 180, 200, 220, 249$ (from bottom to top). Each trace is scaled with its maximum amplitude. Downstream boundary is at $x = 250$ (from Buell & Huerre 1988).

inflectional profiles above low-speed streaks in a boundary layer (see also the models in Huerre 1988).

5. MARGINALLY GLOBALLY STABLE FLOWS

Before discussing examples of globally unstable flows in the next section, we first consider systems that are only marginally globally stable, which means that the highest global mode is only marginally damped [i.e. that the global temporal growth rate of the zeroth mode $\omega_{G0,i}$, defined by Equation (46), is only slightly less than zero]. This situation often arises when a flow is almost absolutely unstable, as shown in Figure 4*c*. One intuitively expects such a system to behave like a slightly damped linear oscillator: If excited at or close to the resonance frequency, a small forcing amplitude of the order of the damping rate produces a large response of order unity.

Using the model equation (18), which has been shown in Section 3 to essentially determine the global behavior, we proceed to establish the analogy between a marginally globally stable, spatially developing flow, and a simple, slightly damped oscillator. Following Monkewitz et al. (1987) and Chomaz et al. (1989b), we adapt the Ginzburg-Landau model as follows. First, a forcing term is added to (18) to represent a concentrated steady-periodic excitation at the station x_f with amplitude f and frequency ω_f:

$$\frac{\partial \psi}{\partial t} - \omega_{kk} k_0 \frac{\partial \psi}{\partial x} - \frac{i}{2}\omega_{kk}\frac{\partial^2 \psi}{\partial x^2} + i\left[\omega_0 + \frac{\omega_{kk}}{2}k_0^2\right]\psi = f\delta(x - x_f)e^{-i\omega_f t},$$

$$|\psi| \to 0 \quad \text{for} \quad |x| \to \infty. \qquad (49)$$

In addition, we use the expansions (30) and (31) of ω_0 and k_0 around ω_s and k_s, respectively, and for the present purpose eliminate the slow variable X according to $X = \varepsilon x$. Next, we characterize the damping rate of the global mode by the small parameter $\mu \ll 1$ and set

$$\begin{aligned} \omega_s &= \omega_{s,r} + i\mu\Omega_{s,i}, \\ \omega_{0XX} &= \omega_{0XX,r} + i\mu\Omega_{0XX,i}, \\ \omega_{kk} &= \omega_{kk,r} + i\mu\Omega_{kk,i}, \\ k_{0X} &= ik_{0X,i} + \mu K_{0X,r}, \end{aligned} \tag{50}$$

where $\Omega_{s,i}$, $\Omega_{0XX,i}$, $\Omega_{kk,i}$, and $K_{0X,r}$, denote given constants of order unity. If we neglect the nonparallel correction $\delta\omega$ in (46), this leads to the zeroth global-mode frequency

$$\begin{aligned} \omega_{G0} &= \omega_{s,r} + (\varepsilon/2)\left[(\omega_{0XX,r}\omega_{kk,r})^{1/2} + k_{0X,i}\omega_{kk,r}\right] + i\mu[\Omega_{s,i} + O(\varepsilon)] \\ &\equiv \omega_{G0,r} + i\mu\Omega_{G0,i}. \end{aligned} \tag{51}$$

To keep matters simple, terms of order $\mu\varepsilon$ have been neglected, and we assume for consistency that $\varepsilon^2 \ll \mu \ll \varepsilon$. Finally, the forcing frequency is chosen close to the "resonance" frequency $\omega_{G0,r}$, and its amplitude is taken to be of order μ:

$$\omega_f = \omega_{G0,r} + \mu\Delta\Omega, \qquad f = \mu F. \tag{52}$$

Equation (49) can now be solved, using the method of multiple scales. From (50) and (51) it is clear that modifications of the global mode with frequency $\omega_{G0,r}$ (to leading order) will occur on the slow time scale $T = \mu t$. The solution is therefore sought in the usual form, with the amplitude function $B(T)$ multiplying the leading-order solution ϕ_1:

$$\begin{aligned} &\psi(x,t) \sim E(x)e^{-i\omega_{G0,r}t}\{B(T)\phi_1(x) + \mu\phi_2\}, \\ &E(x) \equiv \exp\left[i\int_0^x k_0(x')\,dx'\right]. \end{aligned} \tag{53}$$

Inserting (53) into (49) yields, to leading order in μ,

$$\begin{aligned} &\mathscr{L}(\phi_1) \equiv \frac{d^2\phi}{dx^2} + \left[\frac{C^2}{2} - \frac{C^4}{4}(x - x_s)^2\right]\phi = 0, \\ &C \equiv \left[\frac{4\varepsilon^2\omega_{0XX,r}}{\omega_{kk,r}}\right]^{1/4}, \end{aligned} \tag{54}$$

with the solution

$$\phi_1 = \exp(-\xi^2/4)\,\mathrm{He}_0(\xi), \qquad \xi \equiv C(x - x_s), \tag{55}$$

where $He_0 \equiv 1$ is the zeroth Hermite polynomial. This is in essence the mode shape of the highest *free* eigenmode. Its amplitude is determined at the next order in μ by

$$\mathscr{L}(\phi_2) = \frac{-2i}{\omega_{kk,r}}\phi_1\left[\frac{dG}{dT} - \Omega_{s,i}G\right] + FE^{-1}(x)\delta(x-x_f)e^{-i\Delta\Omega T}. \tag{56}$$

Application of a solvability condition and the requirement that the solution be steady periodic leads to the final result

$$B(T) = \frac{FH(x_f)e^{-i\Delta\Omega T}}{\Omega_{s,i} + i\Delta\Omega}, \qquad H(x_f) \equiv iC\omega_{kk,r}(8\pi)^{-1/2}E^{-1}(x_f)\exp(-\xi_f^2/4), \tag{57}$$

which is precisely the response of a slightly damped linear oscillator near resonance, as anticipated. An example for such a slightly damped global mode, maintained by low-level forcing, is the preferred mode in a jet, which is also referred to as the jet-column mode. An operational definition of this mode has been given by Ho & Huerre (1984), for instance, who characterize it in a negative way as not resulting from a subharmonic sequence starting at the jet nozzle. As a consequence, the Strouhal number of the preferred mode is nearly independent of the jet Reynolds number or, equivalently, the initial shear-layer thickness (Figure 14 of Ho & Huerre 1984) and has a value of $St \approx 0.25$ for the two-dimensional jet and $St \approx 0.41$ for the axisymmetric, low-subsonic, top-hat jet.

Monkewitz et al. (1987) have estimated the constants (50) from experimental data in a two-dimensional jet (see Monkewitz 1989a) in order to evaluate $B(T)$ [Equation (57)] and the global-mode shape. The latter is shown in Figure 6 which immediately allows us to conclude that the global-mode amplitude in our doubly infinite domain is very small at the location of the nozzle, which is to the left of where $\omega_{0,i} = \omega_{0,i}|_{max}$. This justifies, a posteriori, omitting the nozzle and at the same time demonstrates the insensitivity of Strouhal number to boundary conditions as a *natural* ingredient of our model. On a quantitative level, Figure 9 shows a comparison between the results from (57) and the conventional approach of evaluating, with locally parallel or slowly diverging theory (see Section 3.1), the total gain experienced by the *spatial* instability wave of frequency ω_f between x_f and its (linear) saturation. From this example it appears that our global-mode approach yields a sharper frequency-selection criterion, more in line with experiments, than the locally parallel theory. Furthermore, the predicted Strouhal number $St = 0.225$ compares very favorably with the experimental value $St = 0.25$.

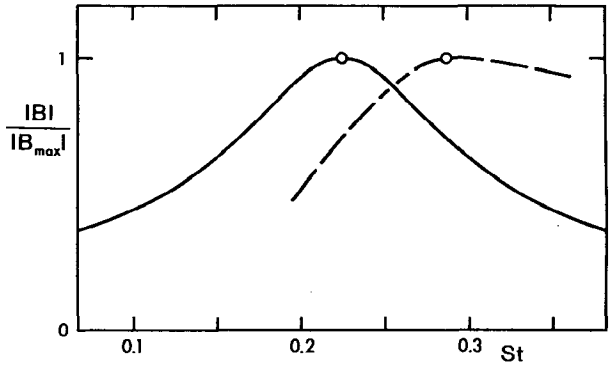

Figure 9 Normalized gain in a two-dimensional jet from Equation (57) (——) and from locally parallel theory (- - - -) (from Monkewitz et al. 1987).

6. EXAMPLES OF GLOBALLY UNSTABLE FLOWS

6.1 *Wakes*

Wake flows have recently served as the pacemaker for research into how local absolute instability can lead to global linear instability and subsequent self-excited nonlinear states. We immediately point out that in most laboratory or numerical experiments, not specifically designed to identify the small-amplitude stages of global instability, one observes only the nonlinear results of the global instability, which are limit-cycle oscillations for the examples considered here.

Although Betchov & Criminale (1966), Mattingly & Criminale (1972), and Nakaya (1976) discovered the existence of branch-point singularities, it was Koch (1985) and Pierrehumbert (1984) who sparked the current interest in these concepts as applied to wake and geophysical flows, respectively, and who explicitly suggested global frequency-selection criteria in terms of local absolute instability (see Section 3.2). Koch's criterion is supported by the numerical simulation of Hannemann & Oertel (1989, their Figure 16). Close agreement is obtained between the saturated von Kármán vortex-shedding frequency and the Koch frequency $\omega_0(X_t)$, with $\omega_{0,r}(X_t) = 0$. This study appears to contradict our claim that Equation (40) is the correct frequency selection criterion. We conjecture that $\omega_{0,r}(X)$ may change only slightly as X varies from X_t to X_s, but we have no definite evidence that this is the case.

Around the same time, Mathis et al. (1984) and, independently, Strykowski (1986) demonstrated in landmark transient experiments that von Kármán vortex shedding at low Reynolds number is the result of a global

instability (see also Provansal et al. 1987, Sreenivasan et al. 1987, 1989b). By impulsively raising the Reynolds number from just below to slightly above the critical value for von Kármán vortex shedding, these authors were able to identify the supercritical Hopf bifurcation to a global mode, the mode's temporal exponential growth in the linear regime, and its final nonlinear saturation in the form of self-sustained oscillations, commonly referred to as the von Kármán vortex street. In addition, they showed that at near-critical conditions the temporal evolution of the characteristic global-mode amplitude is accurately described by a Landau equation (47). The saturation amplitude obtained from (47) by setting $d|B|/dt = 0$ is given by

$$|B|_{\text{sat}} \propto (R - R_{G_c})^{1/2}, \qquad \beta = 0, \qquad R \geq R_{G_c}. \tag{58}$$

The experimental results of Strykowski (1986) displayed in Figure 10 clearly show the exponentially growing (in time) linear global mode to which the analysis of Section 3 applies. This concept of a bifurcation to a global mode has been fully confirmed by Zebib (1987) and Jackson (1987) with global linear stability calculations in which the temporal stability characteristics (ω_G in particular) were determined on the computed non-parallel basic flows.

Monkewitz (1988a) then firmly tied the local stability properties to the observed global behavior by showing that the sequence of transitions in

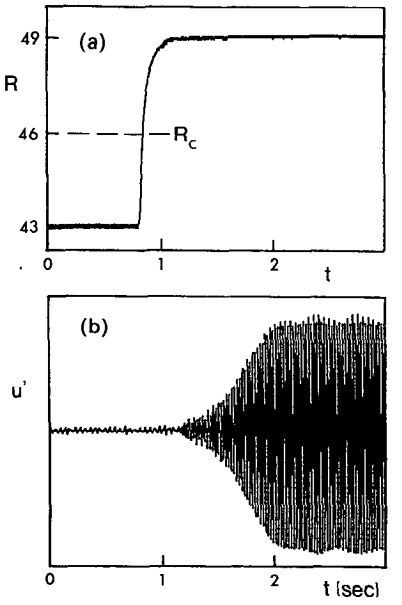

Figure 10 The onset of von Kármán vortex shedding after a step increase of the Reynolds number (from Strykowski 1986, Strykowski & Sreenivasan 1989, with permission). (*a*) mean velocity (low-pass filtered below 30 Hz); (*b*) fluctuating velocity.

the cylinder wake, as the Reynolds number is raised, does indeed follow the sequence in the model problem of Chomaz et al. (1987, 1988; see also 1989a): first, the transition from stability to convective instability, then from convective to local absolute instability, and finally the bifurcation to a self-sustained global mode only after a sufficiently large portion of the flow has become absolutely unstable. We emphasize again that the intermediate transition to local absolute instability is not observable in an experiment, since the concept is based on "fictitious" locally parallel velocity profiles. For the local stability calculations, a two-parameter family of symmetric wake profiles was used with variable wake depth and variable thickness of the mixing layers on both sides of the wake. Matching these analytical profiles to experimental mean velocity profiles, Monkewitz (1988a) found transition to convective instability at a Reynolds number $R^{(D)}$, based on cylinder diameter D and freestream velocity U_∞, of approximately $R^{(D)} \approx 5$; the appearance of the first local absolute instability occurs at $R^{(D)} \approx 25$, long before the onset of von Kármán vortex shedding at the experimentally determined $R^{(D)} = 45$–47, when a substantial portion of the near wake is absolutely unstable.

In the case of a wake, one may think that absolute instability is closely related to the existence of reverse mean flow to "carry information upstream." That such an intuitive concept can be thoroughly misleading is demonstrated by the "floating wake" (Triantafyllou & Dimas 1989) of a circular cylinder immersed half-way into a uniformly flowing stream, as depicted in Figure 11*a*. As shown in Figure 11*b*, these authors demon-

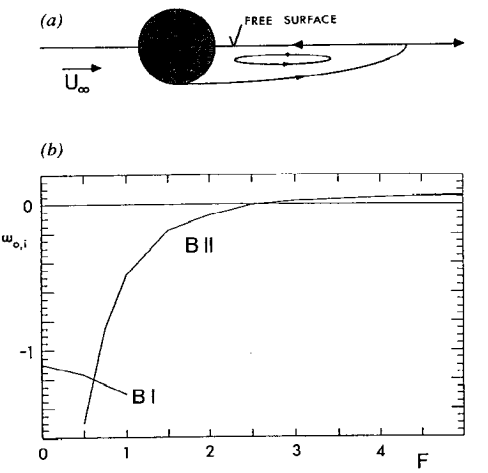

Figure 11 The stability of the floating wake (from Triantafyllou & Dimas 1989, with permission). (*a*) schematic of the mean flow; (*b*) absolute growth rate versus Froude number.

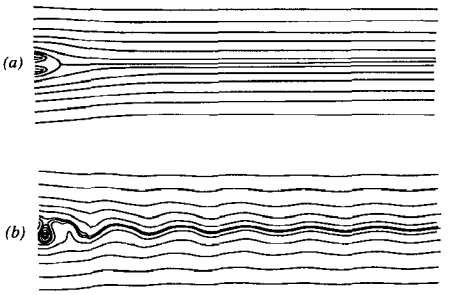

Figure 12 Streamlines of a numerical wake experiment without body at $R = 100$ (courtesy of G. Triantafyllou). (*a*) mean-flow streamlines; (*b*) instantaneous streamlines.

strated that at low Froude number $F = U_\infty(gD/2)^{-1/2}$ the wake is convectively unstable despite the reverse mean flow, whereas in the limit $F \to \infty$ their branch II corresponds to the usual von Kármán mode of a fully immersed cylinder.

On the other hand, the idea that an explanation for von Kármán vortex shedding can be found in the details of the flow separation from the cylinder surface has received a severe blow by an ingenious numerical experiment of G. S. Triantafyllou (private communication). From a computation of the flow around a cylinder that had reached a steady-periodic state, he took the mean velocity profile immediately behind the cylinder and used it as an inflow condition for a second computation without the cylinder. The result was that the flow field (characterized, for instance, by the mean and instantaneous streamlines of Figure 12) was virtually indistinguishable from the original simulation. This lends strong credence to the almost universal practice of simply disregarding the body in wake-stability analyses.

THE EFFECT OF BASE BLEED AND DENSITY VARIATIONS ON VON KÁRMÁN VORTEX SHEDDING The connection between local absolute instability and global self-excitation becomes even more convincing when one looks at the effect of additional parameters, such as base bleed and nonuniform density. For the present purposes the very simplest inviscid and incompressible, two-dimensional wake/jet with uniform velocity and density, bounded by two vortex sheets, provides an excellent qualitative "road map" of these effects. For this simple basic flow the following dispersion relation is obtained in elementary fashion for both the sinuous and the varicose mode, and for variable velocity ratio Λ as well as density ratio S:

$$S\frac{(1+\Lambda-\omega/k)^2}{(1-\Lambda-\omega/k)^2}=\frac{e^k+se^k}{e^k-se^k},$$

$s=+1$: sinuous mode, $s=-1$: varicose mode,

$$\Lambda=(U_{\text{wake/jet}}-U_\infty)/(U_{\text{wake/jet}}+U_\infty), \qquad S=\rho_{\text{wake/jet}}/\rho_\infty. \tag{59}$$

Since we are only interested in the branch points ω_0 that scale with the wake/jet width, we need not be concerned here with the unbounded growth rates as $k\to\infty$. To determine the boundaries between convective and absolute instability in (S,Λ) parameter space, one can take advantage of Equation (59)'s invariance under the transformation

$$S\to S^{-1}, \qquad \Lambda\to-\Lambda, \qquad s\to-s, \tag{60}$$

which is, however, lost for a finite mixing-layer thickness. This leads to the highly symmetric pattern observed in Figure 13, which suggests that reverse flow (i.e. $|\Lambda|>1$) promotes absolute instability as expected, whereas coflow in the case of the jet or base bleed in the wake has the opposite effect. Furthermore, it follows that in the wake it is always the sinuous or von Kármán mode that becomes absolutely unstable first, whereas in the jet it is the varicose or symmetric mode. Lastly, density variations are seen to have the opposite effect in the wake and the jet. While lowering the wake density (in air, for instance, by heating) suppresses absolute instability, it promotes it in the jet. All these three conclusions have been verified experimentally and are illustrated in the following.

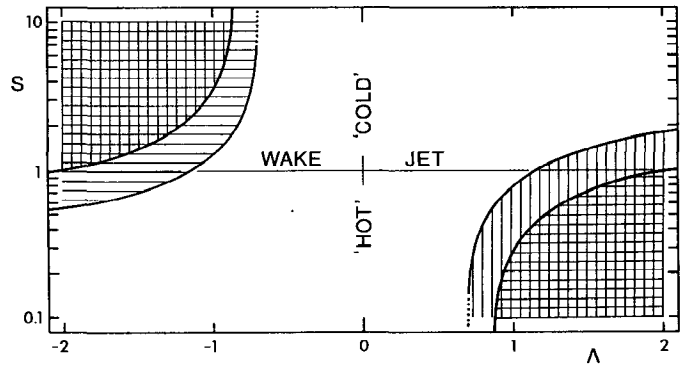

Figure 13 Regions of absolute instability in the (S,Λ)-plane for the sinuous mode (horizontal hatching) and the varicose mode (vertical hatching) in an inviscid, incompressible jet/wake bounded by vortex sheets (from Yu & Monkewitz 1988).

The first example illustrates the effect of base bleed on the global wake stability. Wood (1964) already had demonstrated that a sufficiently large base bleed leads to the suppression of von Kármán vortex shedding behind a blunt airfoil trailing edge, as well as to a substantial drag reduction. His critical bleed coefficient was found by Monkewitz & Nguyen (1987) to be in good agreement with stability calculations showing that the wake is everywhere convectively unstable for $\Lambda > -0.84$. By placing strips of perforated plates (Castro 1971) and screens with different open-area ratios normal to a uniform stream (Inoue 1985), the same effect was demonstrated. The flow-visualization results of Inoue, obtained at the high Reynolds number of $R = 3000$, are reproduced in Figure 14. It is obvious that between an open-area ratio λ of 0.37 and 0.39 an abrupt transition takes place from von Kármán vortex shedding, which is almost indistinguishable from the case $\lambda = 0$, to no von Kármán vortex shedding. This is entirely consistent with the concept of global instability, where the nonlinear saturation amplitude of the observed oscillations increases abruptly according to (58) when the control parameter λ increases beyond a critical value. We also note here that the distinguishing feature between Figures 14*b* and 14*c* is the *near-wake instability*, for which we reserve the term von Kármán vortex shedding. As seen in Figure 14*c*, a convective, sinuous *far-wake instability*, which may be mistaken for a von Kármán vortex street, appears in general farther downstream from the "body." However, it is maintained by external forcing (freestream disturbances, for instance) and hence depends on its level, and it is not "fed" by a self-excited "wavemaker" in the near wake.

Experimentally, other measures, such as the heating of the wake (with air as working fluid), have been found to be effective in suppressing von Kármán vortex shedding (see Table 3). Again, it is possible to relate the effectiveness of heating to changes in local stability properties, as shown qualitatively by Figure 13. More detailed stability calculations for an ideal gas and finite Reynolds number have been carried out by Monkewitz (1988c) and Yu & Monkewitz (1988); they use the family of velocity profiles of Monkewitz & Nguyen (1987) and similar temperature profiles, which is legitimate for a Prandtl number of unity. The resulting boundaries of absolute instability in the (S, R)-plane are shown in Figure 15 for two values of the velocity ratio Λ, as well as for constant and temperature-dependent viscosity. The first conclusion is that the suppression of absolute instability by heating is mainly due to density variations, i.e. to the modification of inertial forces, and not to the modification of viscous forces via the temperature dependence of the viscosity. More precisely, the change of wake density subtly affects the interaction between the two shear layers, which is responsible for the absolute instability in the first place, and leads

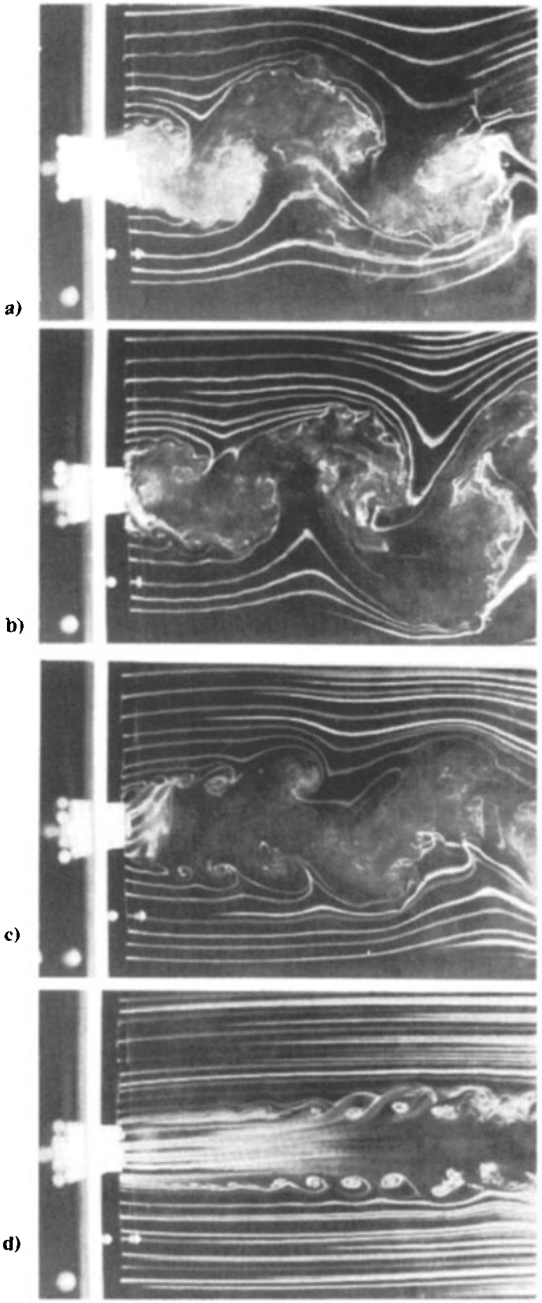

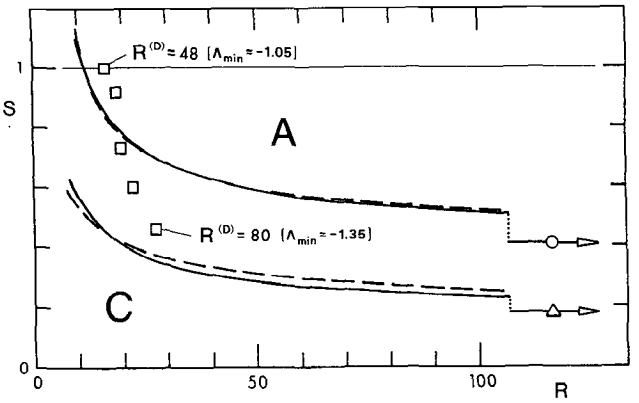

Figure 15 Absolute-instability boundaries of a heated-cylinder wake in the (S, R)-plane for constant (——) and temperature-dependent (- - - -) viscosity, and for velocity ratios of $\Lambda = -1$ (○) and $\Lambda = -1.25$ (△) (from Yu & Monkewitz 1988). □: boundary of global instability (from Berger & Schumm 1988, with permission). A: absolutely unstable domain. C: convectively unstable domain.

to the well-known Strouhal scaling of the von Kármán shedding based on jet width.

Recent experimental data of Berger & Schumm (1988) have also been included in Figure 15. For this purpose, the relationship between the usual Reynolds number $R^{(D)}$ and the pertinent local profile Reynolds number R, based here on the wake half-width and the average between the wake center-line velocity U_c and U_∞, has been estimated according to Monkewitz (1988a). As usual, this step introduces the largest uncertainty into such comparisons. Nevertheless, it appears that again the measured boundary of global instability lies well inside the region of local absolute instability, as suggested by Chomaz et al. (1987, 1988).

OTHER MEASURES AFFECTING VON KÁRMÁN VORTEX SHEDDING In an innovative experiment Strykowski (1986) noticed that von Kármán vortex shedding behind a cylinder could be effectively suppressed by inserting a much smaller "control cylinder" into the flow, immediately outside the wake shear layer. Photographic evidence of this phenomenon at approximately twice the critical Reynolds number both with and without the control cylinder is presented in Figure 16. The effect has been reproduced in a numerical experiment by Strykowski & Sreenivasan (1989), but the relation

Figure 14 Flow past a screen at $R = 3000$ (from Inoue 1985; reprinted with permission of AIAA). (*a*) open-area ratio $\lambda = 0$ (flat plate); (*b*) $\lambda = 0.37$; (*c*) $\lambda = 0.39$; (*d*) $\lambda = 0.55$.

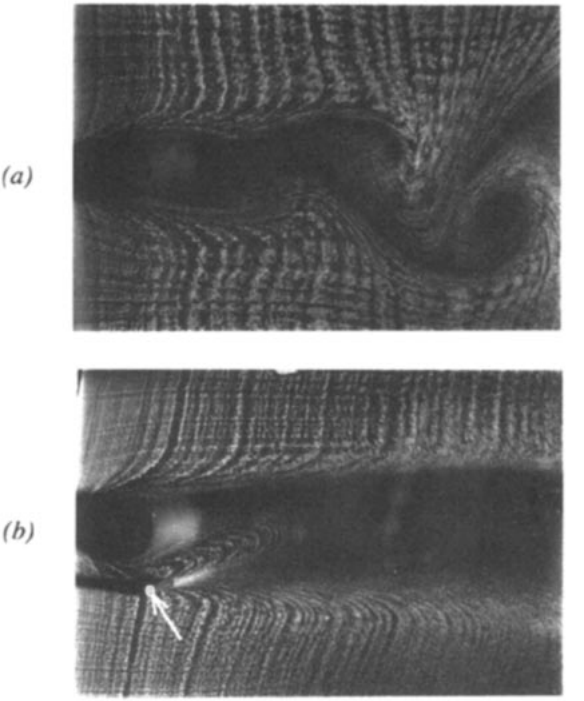

Figure 16 Hydrogen-bubble visualization of (*a*) vortex shedding behind a cylinder at $R = 90$ and (*b*) its suppression by a small "control cylinder" indicated by arrow (from Strykowski 1986, with permission).

of the suppression mechanism to absolute and convective instability of the modified wake has not yet been established. We can only speculate that the asymmetry of the base flow, resulting from the insertion of the control cylinder, may lead to a significant change of local stability properties.

Another method of suppressing the von Kármán vortex street has been devised by Berger (1964, 1967) and Berger & Schumm (1988). It consists of oscillating an oblong cylinder at low amplitude and "high" frequency, in this case slightly less than twice the natural von Kármán frequency. Running the experiment above, but very close to, the critical Reynolds number, these authors were able to show that the forcing amplitude can be used as a control parameter, much in the same way that Reynolds number, base-bleed coefficient, or density ratio can be used. Figure 17 demonstrates the effect by switching the forcing off at t_1, which leads to an exponential growth and subsequent saturation of the von Kármán mode, and by switching it back on at t_2, which leads to the renewed

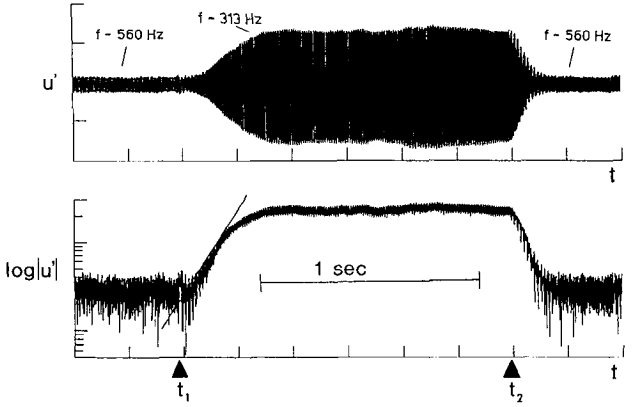

Figure 17 Suppression of vortex shedding behind an oblong cylinder by high-frequency forcing during $t < t_1$ and $t > t_2$ at $R = 81$ ($R_{G_c} = 80$) (from Berger & Schumm 1988, with permission).

suppression of natural vortex shedding. No explanation for this effect is known, and again we can only speculate that it may be related to the weakening of the vortex street by the higher frequency "transition waves" as observed by Bloor & Gerrard (1966) in the cylinder wake around $R^{(D)} \approx 1000$.

6.2 *Low-Density Jets*

Returning to Figure 13, we reiterate that, as opposed to the wake, the low density of the jet promotes absolute instability. This has been verified in detail by the stability calculations of Monkewitz & Sohn (1986, 1988) for the axisymmetric jet and by Yu & Monkewitz (1988) for the two-dimensional, *inertia-dominated* jet. It was also shown that homogeneous incompressible jets are everywhere convectively unstable. In the axisymmetric case, the low-density jet starts to develop a region of local absolute instability below a density ratio $S = \rho_j/\rho_\infty$ of 0.72, where ρ_j is the jet exit density. This first transition to absolute instability is found for zero Mach number and axisymmetric disturbances on a profile near the nozzle, which has a vorticity thickness δ_ω of 8.4% of the jet diameter. Furthermore, the frequency of local modes with zero group velocity scales as a Strouhal number based on the jet diameter, with values between 0.25 and 0.5. In the two-dimensional jet, the corresponding density ratio at which absolute instability first occurs is $S_t = 0.90$.

These findings suggested the possibility of self-sustained global oscillations in low-density jets, exhausting into higher density fluid, and moti-

vated the experiments with an axisymmetric helium-nitrogen jet by Kyle (1988) (see also Sreenivasan et al. 1989a, Kyle & Sreenivasan 1989), with a round, heated air jet by Monkewitz et al. (1988a, 1989a), and with a two-dimensional hot jet by Yu & Monkewitz (1988). Concentrating on the axisymmetric case, both groups indeed observed strong, self-excited oscillations at density ratios below approximately $S \approx 0.6$ in the He/N_2 jet and $S = 0.72$ in the hot-air jet. The experiments indicate that the main requirements for a clean self-excited response are a laminar initial jet shear layer (i.e. a comparatively low Reynolds number) and a very quiet facility. At higher Reynolds and Mach numbers, low-density jets have been found to revert back to the familiar behavior of homogeneous turbulent jets for reasons that are not yet completely understood. To illustrate the limit-cycle oscillator nature of the low-Reynolds-number, low-density jet, we show in Figure 18*a* a typical near-field pressure spectrum of the hot jet. There is little doubt that with its main spectral peak some 30 dB above the background, this spectrum is qualitatively different from that of the homogeneous jet in the same figure. To be positive, however, about the nature of the oscillations—limit-cycle or not—the presence of the (super-critical) Hopf bifurcation to a global mode must be verified by measuring, for instance, the saturation amplitude (58) as a function of the control parameter. This is shown in Figure 18*b*, with the density ratio S playing the role of control parameter. The fact that two modes have been identified is not surprising in light of Section 3's analysis, and this feature does not concern us further.

An interesting aspect of self-excited oscillations in low-density jets is that they have a spectacular effect on the jet spreading, with half-angles occasionally in excess of 45°. This "by-product" of self-excitation is clearly outside the scope of the theoretical stability considerations of Section 3, and it was only discovered during the course of the experiments mentioned above. It is illustrated in Figure 19 for both the helium-nitrogen jet and the hot-air jet. The similarity of the two jets lends further credence to the notion that only the density profile is responsible for the self-excited behavior, as long as buoyancy does not become important close to the nozzle.

Going one step further, Monkewitz et al. (1989c) have found that the large jet spreading under self-excited conditions is highly nonaxisymmetric. They hypothesized that this phenomenon is caused by the Widnall instability of the primary vortex rings and the subsequent radial expulsion of "side jets" by vortex induction. These "side jets" are observed to number between two and six and to roughly coincide with (x, r)-planes that are more or less equally spaced in the azimuthal direction. They are strikingly visualized in Figure 20, which shows two jet cross sections that were produced by placing a laser-sheet perpendicular to the jet axis at $x/D = 3$

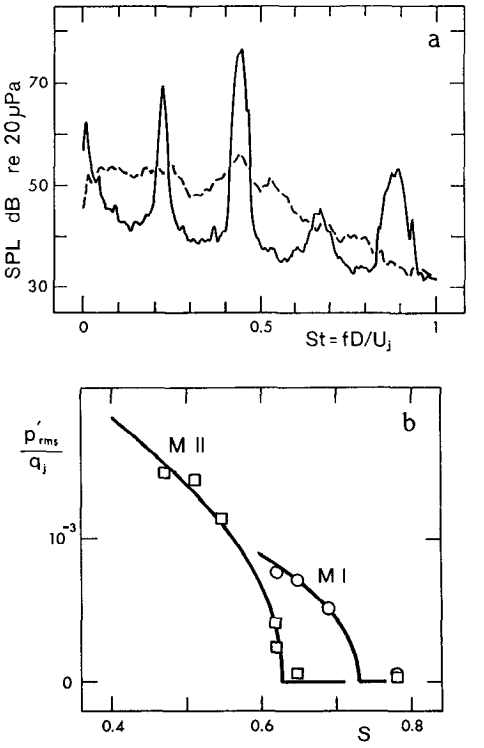

Figure 18 (*a*) Near-field pressure spectrum in a round air jet at $(x/D, r/D) = (0.2, 1.0)$ (from Monkewitz et al. 1989c). ——, hot jet with $S \equiv \rho_e/\rho_\infty = 0.47$ and $R = 7500$; - - - -, cold jet ($S = 1$) of equal dynamic head. (*b*) Amplitude of the dominant near-field pressure oscillation at $R = 7500$, normalized by the jet dynamic head, versus S (from Monkewitz et al. 1989a). ——, Equation (58) fitted to the data.

and then taking a high-speed movie of the light scattered from smoke particles introduced into the jet. Figure 20*a* captures the passage of a primary vortex ring, providing a scale for the side jets, while Figure 20*b* shows the side jets between the passage of primary vortex rings. This property of the low-density jet leads us to believe that on a more general level self-excited oscillations, whether natural or induced by clever manipulation of the flow, may be put to good use, as in many cases they seem to be associated with optimum mixing.

6.3 *Capillary Jets*

The last flow to be specifically discussed in this "zoology" of globally unstable systems is the capillary liquid jet. It serves to show that although the form of the linear global instability is known, its nonlinear result may

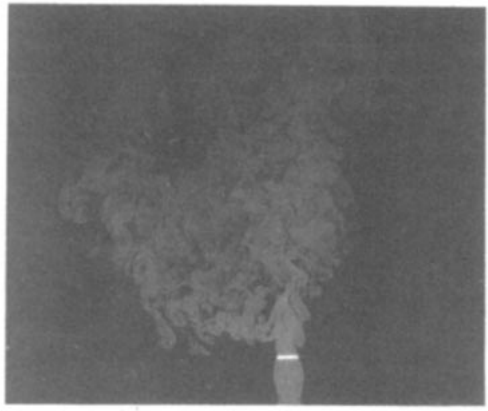

a

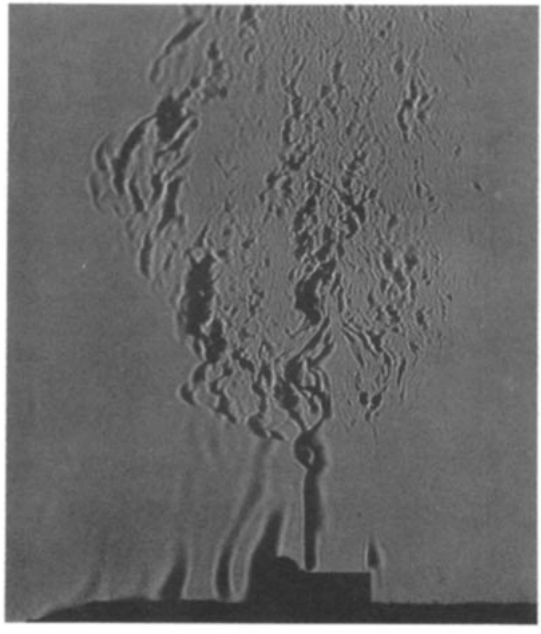

b

Figure 19 (*a*) Side view of helium jet (with $S = 0.14$ and $R = 1400$) by laser-induced fluorescence (from Sreenivasan et al. 1989a). (*b*) Spark-Schlieren of a hot-air jet at $S = 0.56$ and $R = 7500$ (photograph by D. W. Bechert & P. A. Monkewitz).

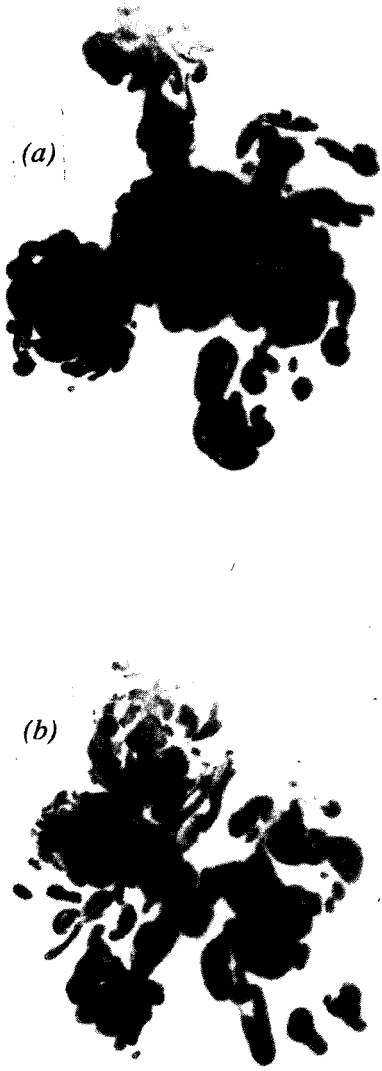

Figure 20 Cross sections of a smoke-seeded hot jet at $x/D = 3$, $S = 0.44$, and $R = 7500$. The photographs, reproduced as negatives, are taken from a high-speed movie (courtesy of B. Lehmann & B. Barsikow).

be quite unexpected. Leib & Goldstein (1986a,b; see also Lin & Lian 1989, Monkewitz et al. 1988b) have demonstrated that on an inviscid basis the Rayleigh instability, which leads to the breakup into drops, becomes absolute when the Weber number W exceeds 0.32 (i.e. when capillary forces become comparable to inertia forces). The Weber number is defined as $W \equiv \sigma/(\rho U^2 r)$, where σ is the liquid surface tension, ρ the jet density, U the uniform jet velocity, and r the jet radius. To investigate the practical effects of absolute instability, Monkewitz et al. (1988b) have carried out experiments covering a range of Weber numbers from 0.06 to about 0.5, with associated Reynolds numbers (based on r_0 and U_0 at the orifice) between approximately 500 and 140.

For each condition the breakup distance was determined between the orifice plate and the location where individual drops formed. It was observed that beyond an initial Weber number W_0 of about 0.3, the breakup distance decreased dramatically and became zero around $W_0 \approx 0.5$ (with $R_0 \approx 180$). Visually, at this critical Weber number the jet goes abruptly from breaking up downstream of the orifice to dripping, without an appreciable change in mean flow rate. The tentative explanation for this behavior is that once the region of absolute instability adjacent to the orifice becomes sufficiently long, a global mode starts growing in time. The resulting finite-amplitude oscillations close to the nozzle presumably then lead to the wetting of the orifice plate and to the formation of large drops. Hence, it may be that the dripping of a faucet is in a broad sense related to von Kármán vortex shedding.

7. FURTHER CONSIDERATIONS

7.1 *Experimental Diagnostics*

A topic of some importance is how to recognize global instability in the laboratory or in a numerical simulation, as the information used in Section 3 for its definition is not generally available. We again emphasize that in this context only the global properties are meaningful, since local absolute instability, which is the property of a fictitious parallel mean flow, cannot in general be directly observed in a spatially developing system. The type of experiments that are suitable for the identification of self-excited global modes can immediately be divided into two classes. The first contains all the "easy" experiments, which address the steady-periodic behavior of the system and in general yield only supporting evidence for the existence of self-excitation. The second class naturally contains the "hard" experiments, which are concerned with the transient behavior of the system as well and yield conclusive proof of self-excitation. A characteristic in

common is the requirement of extremely low uncontrolled external noise so as not to obscure the bifurcation to global modes.

Typical experiments of the first kind are given approximately in ascending order of the strength of the evidence that they can provide. At the very bottom we probably have to place single-point spectral data. Despite the rather convincing look of Figure 18*a*, for instance, it is always possible that a clean spatial instability, especially in a laminar shear flow, can produce an equally peaky spectrum. Next, experiments with steady-periodic forcing should be considered. They can be designed to detect frequency "lock-in" phenomena, which point to a nonlinear oscillator behavior, by sweeping the forcing frequency past a suspected global-mode frequency or its rational multiples (see, for instance, Sreenivasan et al. 1989b). Another design involves the measurement of the system response as a function of forcing amplitude at the suspected global-mode frequency. In the case of a purely convectively unstable system, one expects for small enough forcing a linear relationship between forcing and response amplitude (i.e. the behavior of an "amplifier"), whereas for a self-excited system sufficiently far from critical the saturation amplitude of the limit cycle is insensitive to low-level forcing. This is easily verified with the forced Landau equation (47), which yields $|B|_{sat}(\beta) \approx |B|_{sat}(\beta = 0) + \beta/[2|B|^2_{sat}(\beta = 0)]$ when $\beta \ll |B|^3_{sat}(\beta = 0)$. Around critical conditions, however, the dependence of $|B|_{sat}$ on forcing becomes more pronounced. A typical example of such an experiment is shown in Figure 21. Finally, the measurement of the saturation amplitude as a function of a control parameter, as in Figure 18*b*, generally constitutes strong evidence for the presence of a supercritical Hopf bifurcation. In the case of a subcritical bifurcation the situation becomes far more complicated, however, but we are not aware of any such example.

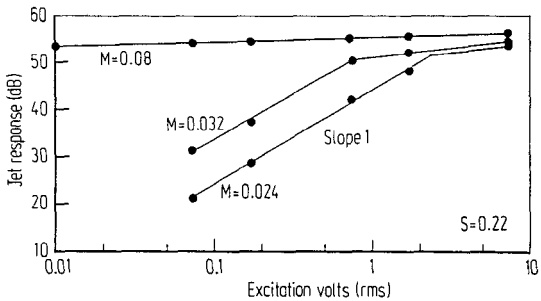

Figure 21 The response of a He/N_2 jet to excitation at $S = 0.22$ and different Mach numbers for a self-excited case (top curve) and two globally stable cases (bottom two curves) (from Sreenivasan et al. 1989a, with permission).

The second class of "hard" experiments is typified by the transient experiment of Mathis et al. (1984), Strykowski (1986), and others. It involves following a global instability in time from its inception, through its small-amplitude linear stage, to saturation. The information obtained in this way at any given point can then be used to evaluate all the complex coefficients of the Landau equation and to positively identify a bifurcation. We may add here that, in order to avoid any misinterpretation, it should be verified that the same Landau equation is satisfied at every point in space.

7.2 *Implications for Flow Control*

The concept of global instability is likely to be fruitful in the context of flow "modification" and "control." Here we reserve the term "control" for closed-loop feedback control, while any other "fiddling" with the flow is referred to as flow "modification." The study of local stability properties—in particular, absolute instability—thereby represents a simple and quick, albeit not foolproof, means of evaluating the global characteristics.

When considering control and flow modification, we must distinguish between two diametrically opposed objectives, which call for very different strategies. The first (and possibly more common) is the suppression, to the greatest extent possible, of all oscillations. The second, equally important objective is the stimulation of a global instability for the purpose of optimal mixing, for instance. This latter task can in general be accomplished very efficiently by a simple, single sensor–single actuator feedback control, as demonstrated experimentally in the homogeneous round jet by Wehrmann (1957) and Reisenthel (1988).

By contrast, the suppression of global instabilities by single sensor–single actuator feedback control in the wake of an oblong cylinder was discovered by Berger (1964, 1967) to be difficult and only possible very close to the natural critical Reynolds number. Both of these situations have been analyzed by Monkewitz (1989a), using the generic Ginzburg-Landau model of Sections 2, 3, and 5. The analysis qualitatively reproduces all the experimental findings and in addition yields the following simple explanation for the success and failure of single sensor–single actuator feedback control: To induce global instability, only a single, and in most applications unspecified, global mode has to be destabilized. To suppress global instability, on the other hand, all global modes must be attenuated. It is clear that in the latter situation, one sensor is in general not sufficient to handle multiple global modes, which often have very closely spaced frequencies [$O(\varepsilon)$ apart in the formulation of Section 3, Equation (46)]. Hence, while the control may be designed to attenuate one mode, it will

in most cases destabilize another, thereby defeating its purpose. Conversely, we speculate that in all examples in which such a simple feedback control works (see, for example, Ffowcs-Williams 1989), there was only a single, self-excited global mode to control, with all others strongly damped. Except under these special circumstances, it therefore appears that the most promising strategy to suppress global instability is to modify the flow system so as to eliminate all regions of absolute instability.

7.3 *Relevance to Chaotic Dynamics*

The classification scheme outlined in the introduction and in Section 3 is particularly pertinent to the study of deterministic chaos in open flows. We recall that in globally unstable flows, a Hopf bifurcation takes place whereby the entire spatial domain is in a limit-cycle state at a natural frequency ω_G. Close to the bifurcation point, the temporal behavior is fully specified by the Landau equation (47). All relevant properties of the unsteady flow field can be characterized by a time series at a single point in space, as is used for closed flows in small-aspect-ratio geometries (Rayleigh-Bénard convection, Taylor-Couette flow). Furthermore the finite-amplitude periodic state reached by globally unstable flows provides a benchmark with which other possible states (tori, strange attractors) can be compared as a control parameter is varied. For instance, if time-harmonic forcing is applied, locked-in regions (Arnold tongues) can be mapped and universal transitions can be identified for particular values of the ratio between the excitation frequency and the natural frequency. Such a program has been carried out experimentally by Olinger & Sreenivasan (1988) for the wake behind an oscillating cylinder and by Sreenivasan et al. (1989a) for a periodically excited helium jet. Numerical simulations of a forced bluff-body wake performed by Karniadakis & Triantafyllou (1989) also reveal the presence of locked-in regions as well as low-dimensional chaotic attractors. In other situations, additional natural frequencies can be introduced by the modes of vibration of the cylinder. The coupling between hydrodynamic and elastic modes may also lead to low-dimensional chaos, as shown by Sreenivasan (1985) and Van Atta & Gharib (1987). We conclude that globally unstable flows are readily amenable to a low-dimensional dynamical-systems approach of the kind used for small-aspect-ratio closed hydrodynamical systems. Complicated spatio-temporal patterns are also possible, as shown by Van Atta et al. (1988).

The dynamical regimes of globally stable flows that are nonetheless locally convectively unstable cannot be as easily characterized. Extreme sensitivity to random external noise makes it difficult to obtain pure limit-

cycle states even when the flow is forced monochromatically. As a result, when the flow is pushed into what appears to be a low-dimensional "chaotic" state, it is often impossible to discriminate between intrinsic chaos and amplification of external random noise (Huerre 1987). To explore other possible approaches, Deissler (1985, 1987a) chose to investigate numerical solutions of the Ginzburg-Landau model with a stabilizing cubic nonlinear term. Under broadband-forcing conditions, the external noise was found to be selectively amplified and spatially growing waves were generated downstream of the source at the frequency of the maximum spatial amplification rate. Farther downstream, however, the nonlinear wave train became modulationally unstable to sidebands. This secondary instability triggered a breakup of the primary finite-amplitude wave into a turbulent state. Random fluctuations in the spatial location of the breakup point were shown to be responsible for intermittency. Since, in the absence of external fluctuations, no spatio-temporal oscillations could be detected, Deissler appropriately coined the term *noise-sustained structures* to describe this phenomenon. Similar dynamics has been identified by Brand & Deissler (1989) in the Kuramoto-Sivashinsky equation. A distinctly different spatio-temporal behavior arises in Ginzburg-Landau models displaying a subcritical bifurcation (destabilizing cubic nonlinearity). As demonstrated by Deissler (1987c), the spatially growing waves generated by random noise produce turbulent spots and slugs that are qualitatively similar to those observed in channel flow and pipe flow. The reader is referred to Deissler (1989) for a survey of recent work in this area.

Few convectively unstable flows have been studied experimentally from a nonlinear dynamical-systems point of view. Experiments on thin airfoil wakes (Aref et al. 1987, Williams-Stuber & Gharib 1989) reveal a wealth of possible flow patterns when several incommensurate frequencies are introduced externally. Bonetti (1988) and Bonetti & Boon (1989) have recently identified low-dimensional chaotic attractors in excited jets with fully developed pipe flow at the nozzle exit plane. The transition to chaos was in this case related to the breakdown of the helical structure generated immediately downstream of the nozzle.

It remains to be established whether the usual statistical measures of chaos, such as Lyapunov exponents, remain applicable in convectively unstable flows. As noticed by Deissler & Kaneko (1987), Lyapunov exponents generated at a fixed spatial location are always negative, a fact presumably related to the negative absolute growth rates prevailing in convectively unstable flows. Deissler & Kaneko propose instead to introduce a velocity-dependent Lyapunov exponent calculated in a frame of reference moving at a constant speed. A convectively unstable flow is then

determined to be chaotic when the maximum value of the Lyapunov exponent over all frame speeds is positive.

7.4 *Relation to Global Instability in Closed Flows*

This review has been centered around spatially developing open flows of infinite streamwise extent. A related question may then be asked: How do local/global and absolute/convective instability concepts carry over to flows in finite geometries that, in their basic state, are spatially homogeneous? In the last five years, important advances have been made in our understanding of traveling-wave states in closed flows, the primary objective being the description of spatio-temporal complexity in convecting binary fluid mixtures. The most successful model appears to be that proposed by Cross (1986, 1988) for finite systems exhibiting an instability to an oscillating spatially periodic state with $x \to -x$ symmetry. Cross considers two coupled Ginzburg-Landau equations with constant coefficients governing the amplitudes ψ_L and ψ_R of left- and right-moving waves (see also Coullet et al. 1985). As a control parameter R is varied, the linearized system undergoes successive transitions from stable to convectively unstable to absolutely unstable, as sketched in Figures 1*f,g,h*. Numerical simulations reveal that in convectively unstable situations (Figure 1*g*), the finite-size nonlinear system admits "*confined traveling-wave states*" that are restricted to one side of the spatial domain, namely right-moving waves on the right side or left-moving waves on the left side. In contrast with open infinite systems, global modes can therefore exist in finite geometries even though the medium is convectively unstable everywhere. In a subrange of control parameters, more complicated "blinking states" are also possible, which consist of left- and right-moving traveling waves periodically alternating between either side of the cell. As the basic state becomes absolutely unstable everywhere (Figure 1*h*) there is a distinct transition to a *full-cell nonlinear saturated state* composed of counter-propagating traveling waves. Thus, the occurrence of absolute instability in this class of closed flows signals the onset of a global mode occupying the full length of the system. It is striking that the detailed sequence of nonlinear states predicted by Cross (1988) has been confirmed by many careful experimental studies of binary fluid convection. In particular, confined traveling-wave states have been observed and documented by Heinrich et al. (1987) and Moses et al. (1987), blinking states by Fineberg et al. (1988) and Kolodner & Surko (1988), and full-cell saturated nonlinear traveling-wave states by Walden et al. (1985) and Moses & Steinberg (1986). Recent experimental progress has been extensively discussed by

Kolodner et al. (1989) and Steinberg et al. (1989). Not all global or confined states can be explained in terms of the local nature of the instability in open flows and closed flows: Recent experiments by Bensimon et al. (1989) in binary fluid convection in an annulus do show the existence of stable confined states that cannot be related to local instability properties.

7.5 *Pattern Propagation Fronts*

The theoretical considerations outlined in this review bear a close relationship with the determination of the front propagation velocity of a pattern into an unstable basic state. When a localized perturbation is initiated in a spatially uniform unstable state, a linear wave packet develops, as sketched in Figure 1. In the nonlinear regime, a pattern is then generated that spreads out into the unstable state. The front separating the nonlinear pattern from the unstable basic state propagates at a well-defined velocity V_F, and a particular complex wave number k_F is selected by the dynamics immediately behind the front. Dee & Langer (1983), Ben-Jacob et al. (1985), and Shraiman & Bensimon (1985) have proposed a selection principle for V_F and k_F that is based on linear marginal-stability arguments. More specifically, the velocity V_F and the wave number k_F are such that, in a reference frame moving with the front, perturbations are neutrally stable. From Figure 1, it is then immediately obvious that the fronts coincide with the specific rays $x/t = V_F$ where the growth rate $\sigma \equiv \omega_i(k_*) - (x/t)k_{*i}$ is identically zero. Thus, in the notation of this review, the Dee-Langer criterion for V_F and k_F can be stated as

$$\frac{\partial \omega}{\partial k}(k_F) = V_F, \tag{61}$$

$$\sigma \equiv \omega_i(k_F) - V_F k_{F,i} = 0. \tag{62}$$

For instance, application of this criterion to the linearized Ginzburg-Landau equation (8) yields the front velocities

$$V_F = \omega_k \pm |\omega_{kk}| \left[\frac{-2\omega_{Ri}(R - R_c)}{\omega_{kk_i}} \right]^{1/2}. \tag{63}$$

These values correspond to the slopes of the rays delineating the extent of the wave packet in Figure 1. They have recently been derived by Niklas et al. (1989). The predictions of the Dee-Langer criterion have been verified experimentally (Ahlers & Cannell 1983) and numerically (Luecke et al.

1984, 1985) for the propagation front separating a pattern of Taylor vortices from the ambient unstable Couette flow. Excellent agreement has been obtained by Fineberg & Steinberg (1987) in the case of a convection roll pattern invading the conduction state in Rayleigh-Bénard cells. In both cases, the particular version of the Ginzburg-Landau equation associated with a stationary bifurcation was chosen to predict the front velocity. More recent theoretical work by Ben-Jacob et al. (1985) and Van Saarlos (1988, 1989) indicates that the linear marginal-stability criterion only holds in systems undergoing a supercritical bifurcation with a continuous transition to a finite-amplitude state. When the bifurcation is subcritical, pattern propagation into the unstable state follows a nonlinear marginal-stability criterion.

ACKNOWLEDGMENTS

We wish to thank J. M. Chomaz, A. Michalke, and L. G. Redekopp for their helpful comments and kind encouragement. We also appreciate the assistance of G. Dwinell, D. Erwin, and J. Maes in preparing the manuscript.

This work was supported by the Air Force Office of Scientific Research under Grants F49620-85-C-0080 (PH & PAM) and 87-0329 (PAM) and by ATT under Contract No. ATT-Redekopp (PH).

APPENDIX: SUMMARY OF RESULTS FOR DIFFERENT TYPES OF FLOW

Glossary of acronyms and parameters

LS: linear stability analysis
LE: laboratory experiment
NE: numerical experiment
CI: convective instability
AI: absolute instability
GLI: global instability
Λ: velocity ratio
S: density ratio
R: Reynolds number
M: Mach number
F: Froude number
W: Weber number

Table 1 Wall-bounded shear flows

System	Characteristic parameters	Type of investigation	Results and references
Flat plate boundary layer	Blasius boundary-layer profile, $M \approx 0$	Local LS and global behavior by LE	* Impulse response implying CI (Gaster 1965, 1968, 1975) * Experimental verification of global stability by measuring impulse response (Gaster & Grant 1975)
Flat plate boundary-layer	Instantaneous velocity profiles measured in the transition region, $M \approx 0$	Kinematic wave theory and local LS of secondary instabilities	* Self-excitation of secondary instability, implying its AI character (Landahl 1972)
Flat plate boundary-layer	Blasius boundary-layer profile, $M \approx 0$	Local LS	* CI, focus on signaling problem (receptivity to sound) (Tam 1981)

Flat plate boundary-layer	Blasius boundary-layer profile, $M = 0$	Local LS	* No AI found; role of continuous spectrum in the impulse response (Ashpis & Reshotko 1989)
Plane Poiseuille flow	$M = 0$, all R	Local LS	* CI at all R (Deissler 1987b) * Direct spatial resonances (Koch 1986)
Boundary-layer on a concave wall	Asymptotic suction profile, $M = 0$	Local LS	* CI for the primary Görtler instability (Park & Huerre 1988)
Boundary-layer on rotating disk	$249 < R < 570$, $M \approx 0$, disk with roughness element	Global behavior by LE and local LS	* Wave packet originating from roughness element, implying CI (Wilkinson & Malik 1985, Mack 1985, Reed & Saric 1989)
Boundary-layer over compliant wall	$M = 0$, $R = \infty$ and finite	Local LS	* AI above critical freestream velocity (Brazier-Smith & Scott 1984, Carpenter & Garrad 1986)

Table 2 Single mixing layers[a]

System	Characteristic parameters	Type of investigation	Results and references
Plane mixing layer	Tanh (y) velocity profile, $R = \infty$, $S = 1$, $M = 0$, variable Λ	Local LS	* AI for $\Lambda \geq 1.315$ (Huerre & Monkewitz 1985)
Plane mixing layer	Broken-line velocity profile, $R = \infty$, $S = 1$, $M = 0$, variable Λ	Local LS	* AI for $\Lambda \geq 1$ (Balsa 1987) * Receptivity problem for $\Lambda < 1$ and a line source (Balsa 1988)/point source (Balsa 1989)
Plane compressible mixing layer	Tanh (y) velocity profile, $R = \infty$, $M \neq 0$, $\Lambda = 1$	Local LS	* CI, focus on signaling problem (receptivity to sound) (Tam 1978)
Inhomogeneous plane mixing layer	Tanh (y) velocity profile, $R = \infty$, $M \neq 0$, variable S, variable Λ	Local LS	* Boundary between CI and AI in (M, S, Λ) parameter space (Pavithran & Redekopp 1989, Djordjevic et al. 1989, Jackson & Grosch 1989)

Plane mixing layer	$M = 0$, $\Lambda = \infty$ as well as variable	Global behavior by LE	* Tilting-tank experiment with $\Lambda = \infty$ shows (temporal) AI (Thorpe 1971) * Extension to variable Λ (Ramshankar 1986)
Plane mixing layer	$M = 0$	Global behavior by NE	* Discovery of self-excited global modes due to feedback from downstream to upstream end of computational box (Lowery & Reynolds 1986, Buell & Huerre 1988)
Inhomogeneous plane mixing layer with wake component	Tanh (y) velocity profile plus Gaussian wake, tanh (y) density profile, $R = \infty$, $M = 0$, variable S, variable Λ	Local LS (spatial)	* Probable AI for $\Lambda = 0.45$ and $S <$ approx. 0.12 * Direct resonance between shear layer and wake mode (Koochesfahani & Frieler 1987)
Inhomogeneous plane mixing layer with buoyancy	Stable stratification with gravity normal to the flow, $R = \infty$, $M = 0$, variable S, variable Λ	Local LS	* For Λ corresponding to AI in the homogeneous case, increasing Richardson number leads to loss of AI (Lin & Pierrehumbert 1986)

[a] Definition of parameters: $\Lambda = (U_1 - U_2)/(U_1 + U_2)$, velocity ratio of streams (1) and (2); $S = \rho_1/\rho_2$, density ratio of streams (1) and (2).

Table 3 Wakes[a]

System	Characteristic parameters	Type of investigation	Results and references
2-D wake	Sech^2 (y) velocity profile, $R = \infty$, $S = 1$, $M = 0$, variable Λ	Local LS	* AI for $\Lambda \leq -0.904$ and the von Kármán mode (Betchov & Criminale 1966, Mattingly & Criminale 1972, Monkewitz & Nguyen 1987)
2-D wake	Family of velocity profiles pertinent to wake of blunt trailing edge, $R = \infty$, $S = 1$, $M = 0$, variable Λ	Local LS	* AI in the near wake (Koch 1985) * Postulate of global frequency-selection criterion $\omega_G = \omega_0(X_t)$, where $\omega_{0,t}(X_t) = 0$
2-D wake	Broken-line, measured cylinder wake profiles and family of velocity profiles, $R = \infty$, $S = 1$, $M = 0$, variable Λ	Local LS	* AI for near-wake profiles corresponding to von Kármán shedding (Triantafyllou et al. 1986, 1987) * Boundary of AI in (Λ, profile shape parameter)-space for von Kármán and varicose mode (Monkewitz & Nguyen 1987)
2-D wake	Family of velocity profiles and computed profiles, finite R, $M = 0$, $S = 1$, variable Λ	Local LS	* AI for $R >$ approx. 45 in the sech^2 (y) wake with $\Lambda = -1$ (Nakaya 1976) * Boundary of AI in (Λ, R)-space for Gaussian wake (Hultgren & Aggarwal 1987) * Boundary of AI in (Λ, R, profile shape parameter)-space. Evidence of AI region before GLI by comparison with measured profiles (Monkewitz 1988a) * Evidence of AI region before GLI by comparison with computed profiles (Hannemann 1988, Hannemann & Oertel 1989, Yang & Zebib 1989)
2-D cylinder wake	$M \approx 0$, R near the onset of von Kármán vortex shedding	Global behavior by transient LE (step change of R)	* Discovery of supercritical Hopf bifurcation leading to GLI (Mathis et al. 1984, Provansal et al. 1987, Strykowski 1986, Sreenivasan et al. 1987, 1989b)

2-D oblong cylinder wake	$M \approx 0$, R near the onset of von Kármán vortex shedding, oscillating cylinder (in feedback loop or open loop at "high" frequency)	Global behavior by transient LE (switch-on/off of cylinder oscillations)	* Suppression of von Kármán vortex shedding by cylinder oscillations (Berger 1964, 1967; mathematical modeling by Monkewitz 1989a) * Demonstration of GLI (Berger & Schumm 1988, Berger 1989)
2-D wake of blunt trailing edge	$M \approx 0$, R near the onset of von Kármán vortex shedding, variable base blowing/suction	Global behavior by transient LE (step change of base bleed)	* Suppression of von Kármán vortex shedding by steady base bleed at high R (Wood 1964) * Demonstration of GLI (Berger 1989)
2-D wake behind strips of screen and perforated plate	$M \approx 0$, $S = 1$, R from 3×10^3 to 9×10^4	Global behavior by LE and NE	* Suppression of von Kármán vortex shedding (GLI) for sufficiently large open-area ratio (Castro 1971, Inoue 1985)
2-D wake of variously shaped cylinders	$M = 0$, $S = 1$, R near the onset of von Kármán vortex shedding	Global LS	* Critical R for GLI (Hopf bifurcation) (Zebib 1987, Jackson 1987)
2-D wake of blunt trailing edge	$M = 0$, $S = 1$, different R, provision for base bleed	Global behavior by NE	* Demonstration of GLI and its suppression by base bleed (Hannemann 1988, Hannemann & Oertel 1989, Karniadakis & Triantafyllou 1989)
2-D compressible wake of flat plate	$M \neq 0$ including $M > 1$, plate surface with variable roughness	Global behavior by LE and local LS	* Suggestion of GLI based on AI for certain parameters (Althaus et al. 1988)
2-D heated-cylinder wake	$M \approx 0$, $S \neq 1$, variable R mostly near the onset of von Kármán vortex shedding	Global behavior by LE	* Suppression of vortex shedding by heating (Noto et al. 1985, Mori et al. 1986, Strykowski 1986, Strykowski & Sreenivasan 1989, Berger & Schumm 1988, Lecordier et al. 1988)
2-D inhomogeneous (heated) wake	Family of velocity profiles, $M = 0$, $S \neq 1$, $F = \infty$, variable R and Λ	Local LS	* Boundary of AI in (S, R, Λ)-plane with CI for sufficiently low S (Monkewitz 1988c)
2-D cylinder wake with control cylinder	$46 < R < 100$, $M \approx 0$, $S = 1$	Global behavior by LE and NE	* Suppression of GLI by presence of small cylinder in near wake (Strykowski 1986, Strykowski & Sreenivasan 1989)

Table 3 Wakes[a] (*continued*)

System	Characteristic parameters	Type of investigation	Results and references
2-D wake of floating bluff body	Measured velocity profiles, $M = 0$, $S = 1$, $R = \infty$, variable F	Local LS	* CI for $F < F_{crit}$, otherwise AI (Triantafyllou & Dimas 1989)
Wake of axisymmetric disk	$1.5 \times 10^4 < R < 3.5 \times 10^5$, $M \approx 0$, $S = 1$	Global behavior by LE	* Lock-on of helical vortex shedding, suggesting GLI (Scholz 1986)
Axisymmetric wake	Family of velocity profiles, $M = 0$, $S = 1$, variable R and Λ	Local LS	* AI for first helical mode only * Boundary of AI in (R, Λ, profile shape parameter)-space (Monkewitz 1988b)
Sphere wake	$M = 0$, $S = 1$, variable R	Global LS	* GLI (Hopf bifurcation) at $R = 175$ (Kim & Pearlstein 1989)

[a] Definition of parameters: $\Lambda = (U_c - U_\infty)/(U_c + U_\infty)$, velocity ratio of centerline (c) and freestream velocity (∞); $S = \rho_c/\rho_\infty$, density ratio.

Table 4 Jets[a]

System	Characteristic parameters	Type of investigation	Results and references
Axisymmetric jet	Vortex sheet, $R = \infty$, $\Lambda = 1$, $F = \infty$, variable M and S	Local LS	* CI for examples with $1.6 < M < 3.8$ (Tam 1971) * AI for $M = 0$ and $S \leq 0.6$ and axisymmetric mode (Michalke 1970, Huerre & Monkewitz 1985)
Axisymmetric jet	Family of velocity and density profiles, $R = \infty$, $F = \infty$, variable M, Λ, and S	Local LS	* Spatial stability, implying AI for $S = 0.5$ (Michalke 1971, 1984) * Boundary of AI in (M, Λ, S, profile shape parameter)-space. $S_{max} = 0.72$ for AI at $M = 0$ (Monkewitz & Sohn 1986, 1988)

Heated axisymmetric jet	$5 \times 10^3 < R < 5 \times 10^4$, $0.03 < M < 0.3$, $\Lambda = 1$, variable S	Global behavior by LE	* Demonstration of GLI as function of S and R (or M), and presence of Hopf bifurcation (Monkewitz et al. 1988a, 1989a) * Implications for entrainment (Monkewitz et al. 1989c)
Inhomogeneous axisymmetric jet	$0.02 < M < 0.5$, $\Lambda = 1$, variable S (He-N_2 mixture)	Global behavior by LE	* Demonstration of GLI as function of S and M, lock-on to forcing, and effect on spreading (Kyle 1988, Sreenivasan et al. 1989a, Kyle & Sreenivasan 1989, Guyon 1988) * Indication of GLI in dump combustor (Subbarao 1987)
Axisymmetric jet with feedback	$3.9 \times 10^4 < R < 8.5 \times 10^4$, $M \approx 0$, $\Lambda = 1$, $S = 1$, feedback from hot wire to acoustic driver	Global LS (model)	* Demonstration of GLI for feedback gains $G > G_{crit}$ (Reisenthel 1988; generic modeling by Monkewitz 1989a)
2-D jet	Family of velocity profiles fitted to experiment, $R = \infty$, $M = 0$, $\Lambda = 1$, $S = 1$	Global LS (model)	* Association of jet-column mode with excited global mode for marginal global stability (Monkewitz et al. 1987, 1989b)
2-D inhomogeneous jet	Family of velocity and density profiles, $R = \infty$, $M = 0$, $\Lambda = 1$, $F = \infty$, variable S	Local LS	* Boundary of AI in (S, profile shape parameter)-space. $S_{max} = 0.90$ for AI (Monkewitz 1988c, Yu & Monkewitz 1988)
Axisymmetric capillary jet	Uniform velocity and parabolic profiles, $R = \infty$ and finite, $S = \infty$ and finite, variable W	Local LS	* AI for large enough surface-tension effects. Boundary of AI in (W, S, R, profile shape parameter)-space (Leib & Goldstein 1986a,b, Lin & Lian 1989, Monkewitz et al. 1988b)
Axisymmetric capillary jet	$100 < R < 500$, $0.08 < W < 0.5$	Global behavior by LE	* GLI with large enough region of AI. GLI manifested by dripping (Monkewitz et al. 1988b)

[a] Definition of parameters: $\Lambda = (U_{c/j} - U_\infty)/(U_{c/j} + U_\infty)$, velocity ratio of centerline (c) or jet exit (j) and freestream velocity (∞); $S = \rho_{c/j}/\rho_\infty$, density ratio.

Literature Cited

Ahlers, G., Cannell, D. S. 1983. Vortex-front propagation in rotating Couette-Taylor flow. *Phys. Rev. Lett.* 50: 1583–86

Akhiezer, A. I., Polovin, R. V. 1971. Criteria for wave growth. *Sov. Phys. Usp.* 14: 278–85

Althaus, W., Limberg, W., Krause, E. 1988. Vortex formation in the wake of a flat plate for subsonic and supersonic free stream Mach numbers. *Phys. Compres. Turbul. Mixing, Princeton, N.J.* (Abstr.)

Ashpis, D., Reshotko, E. 1989. The vibrating ribbon problem revisited. Submitted for publication

Aref, H., Gharib, M., Van Atta, C. W. 1987. Chaos in shear flows. *AIAA Pap. No. 87-1251*

Balsa, T. F. 1987. On the spatial instability of piecewise linear free shear layers. *J. Fluid Mech.* 174: 553–63

Balsa, T. F. 1988. On the receptivity of free shear layers to two-dimensional external excitation. *J. Fluid Mech.* 187: 155–77

Balsa, T. F. 1989. Three-dimensional wave packets and instability waves in free shear layers and their receptivity. *J. Fluid Mech.* 201: 77–97

Bar-Sever, Y., Merkine, L. O. 1988. Local instabilities of weakly non-parallel large-scale flows: WKB analysis. *Geophys Astrophys. Fluid Dyn.* 41: 233–86

Bechert, D. W. 1985. Excitation of instability waves. *Z. Flugwiss. Weltraumforsch.* 9: 356–61

Ben-Jacob, E., Brand, H. R., Dee, G., Kramer, L., Langer, J. S. 1985. Pattern propagation in nonlinear dissipative systems. *Physica D* 14: 348–64

Bensimon, D., Kolodner, P., Surko, C. M., Williams, H., Croquette, V. 1989. Competing and coexisting dynamical states of traveling-wave convection in an annulus. Submitted for publication

Berger, E. 1964. Unterdrueckung der laminaren Wirbelstroemung und des Turbulenzeinsatzes der Kármánschen Wirbelstrasse im Nachlauf eines schwingenden Zylinders bei kleinen Reynoldszahlen. In *Jahrbuch der Wissenschaftlichen Gesellschaft fuer Luft- und Raumfahrt (WGLR)*, pp. 164–72. Braunschweig: Friedr. Vieweg & Sohn

Berger, E. 1967. Suppression of vortex shedding and turbulence behind oscillating cylinders. *Phys. Fluids* 10: 191–93 (Suppl.)

Berger, E. 1989. Paper presented at ONR Workshop Bluff-Body Near-Wake Instab., Lehigh Univ., Bethlehem, Pa.

Berger, E., Schumm, M. 1988. Untersuchungen der Instabilitaetsmechanismen im Nachlauf von Zylindern. *Contract. Rep. No. Be 343/18-1*, Tech. Univ., Berlin, Germ.

Bers, A. 1975. Linear waves and instabilities. In *Physique des Plasmas*, ed. C. DeWitt, J. Peyraud, pp. 117–215. New York: Gordon & Breach

Bers, A. 1983. Space-time evolution of plasma instabilities—absolute and convective. In *Handbook of Plasma Physics*, ed. M. N. Rosenbluth, R. Z. Sagdeev, 1: 451–517. Amsterdam: North-Holland

Betchov, R., Criminale, W. O. 1966. Spatial instability of the inviscid jet and wake. *Phys. Fluids* 9: 359–62

Bloor, M. S., Gerrard, J. H. 1966. Measurements of turbulent vortices in a cylinder wake. *Proc. R. Soc. London Ser. A* 294: 319–42

Bonetti, M. 1988. *Dynamique chaotique dans les écoulements ouverts: le jet excité*. DSc thesis. Univ. Bruxelles, Brussels, Belg.

Bonetti, M., Boon, J. P. 1989. Chaotic dynamics in open flow: the excited jet. *Phys. Rev. A*. In press

Brand, H. R., Deissler, R. J. 1989. Noise-sustained structures in the Kuramoto-Sivashinsky equation. *Phys. Rev. A* 39: 462–65

Brazier-Smith, P. R., Scott, J. F. 1984. Stability of fluid flow in the presence of a compliant surface. *Wave Motion* 6: 547–60

Briggs, R. J. 1964. *Electron-Stream Interaction With Plasmas*. Cambridge, Mass: MIT Press

Buell, J. C., Huerre, P. 1988. Inflow/outflow boundary conditions and global dynamics of spatial mixing layers. *Proc. NASA Ames/Stanford Cent. Turbul. Res. Summer Program. Rep. No. CTR-S88*, pp. 19–27

Cap, F. F. 1976. *Handbook of Plasma Instabilities*, Vol. 1, Chap. 10. New York: Academic

Carpenter, P. W., Garrad, A. D. 1986. The hydrodynamic stability of flow over Kramer-type compliant surfaces. Part 2. Flow-induced surface instabilities. *J. Fluid Mech.* 170: 199–232

Castro, I. P. 1971. Wake characteristics of two-dimensional perforated plates normal to an air-stream. *J. Fluid Mech.* 46: 599–609

Chomaz, J. M., Huerre, P., Redekopp, L. G. 1987. Models of hydrodynamic resonances in separated shear flows. *Proc. Symp. Turbul. Shear Flows, 6th, Toulouse, Fr.*, pp. 3.2.1–6

Chomaz, J. M., Huerre, P., Redekopp, L. G. 1988. Bifurcations to local and global modes in spatially-developing flows. *Phys. Rev. Lett.* 60: 25–28

Chomaz, J. M., Huerre, P., Redekopp, L. G. 1989a. A frequency selection criterion in spatially-developing flows. Submitted for publication

Chomaz, J. M., Huerre, P., Redekopp, L. G. 1989b. Effect of nonlinearity and forcing on global modes. *Proc. Conf. New Trends in Nonlinear Dyn. and Pattern-forming Phenom.*, ed. P. Coullet, P. Huerre. New York/London: Plenum. In press

Clemmow, P. C., Dougherty, J. P. 1969. *Electrodynamics of Particles and Plasmas*. Reading, Mass: Addison-Wesley

Coullet, P., Fauve, S., Tirapegui, E. 1985. Large scale instability of nonlinear standing waves. *J. Phys. (Paris) Lett.* 46: 787–91

Crighton, D. G., Gaster, M. 1976. Stability of slowly-diverging jet flow. *J. Fluid Mech.* 77: 397–413

Cross, M. C. 1986. Traveling and standing waves in binary fluid convection in finite geometries. *Phys. Rev. Lett.* 57: 2935–38

Cross, M. C. 1988. Structure of nonlinear travelling-wave states in finite geometries. *Phys. Rev. A* 38: 3592–3600

Davis, S. H. 1976. The stability of time-periodic flows. *Annu. Rev. Fluid Mech.* 8: 57–74

Dee, G., Langer, J. S. 1983. Propagating pattern selection. *Phys. Rev. Lett.* 50: 383–86

Deissler, R. J. 1985. Noise-sustained structure, intermittency, and the Ginzburg-Landau equation. *J. Stat. Phys.* 40: 371–95

Deissler, R. J. 1987a. Spatially-growing waves, intermittency and convective chaos in an open-flow system. *Physica D* 25: 233–60

Deissler, R. J. 1987b. The convective nature of instability in plane Poiseuille flow. *Phys. Fluids* 30: 2303–5

Deissler, R. J. 1987c. Turbulent bursts, spots and slugs in a generalized Ginzburg-Landau equation. *Phys. Lett.* 120: 334–40

Deissler, R. J. 1989. External noise and the origin and dynamics of structure in convectively unstable systems. *J. Stat. Phys.* 54: 1459–88

Deissler, R. J., Brand, H. R. 1988. Generation of counter-propagating nonlinear interacting traveling waves by localized noise. *Phys. Lett.* 130: 293–98

Deissler, R. J., Kaneko, K. 1987. Velocity-dependent Lyapunov exponents as a measure of chaos for open-flow systems. *Phys. Lett.* 119: 397–401

Dimotakis, P. E., Brown, G. L. 1976. The mixing layer at high Reynolds number: large-structure dynamics and entrainment. *J. Fluid Mech.* 78: 535–60

Djordjevic, V., Pavithran, S., Redekopp, L. G. 1989. Stability properties of subsonic mixing layers. *AIAA Pap. No. 89-1020*

Fainberg, Ya. B., Kurilko, V. I., Shapiro, V. D. 1961. Instabilities in the interaction of charged particle beams with plasmas. *Sov. Phys. Tech. Phys.* 6: 459–63

Ffowcs-Williams, J. E. 1989. Control of unsteady flows. *AIAA Pap. No. 89-0990*

Fineberg, J., Moses, E., Steinberg, V. 1988. Spatially and temporally modulated traveling wave pattern in convecting binary mixtures. *Phys. Rev. Lett.* 61: 838–41

Fineberg, J., Steinberg, V. 1987. Vortex front propagation in Rayleigh-Bénard convection. *Phys. Rev. Lett.* 58: 1332–35

Fuchs, V., Ko, K., Bers, A. 1981. Theory of mode-conversion in weakly inhomogeneous plasma. *Phys. Fluids* 24: 1251–61

Gaster, M. 1965. On the generation of spatially growing waves in a boundary layer. *J. Fluid Mech.* 22: 433–41

Gaster, M. 1968. Growth of disturbances in both space and time. *Phys. Fluids* 11: 723–27

Gaster, M. 1975. A theoretical model of a wavepacket in the boundary layer on a flat plate. *Proc. R. Soc. London Ser. A* 347: 271–89

Gaster, M., Grant, I. 1975. An experimental investigation of the formation and development of a wavepacket in a laminar boundary layer. *Proc. R. Soc. London Ser. A* 347: 253–69

Gaster, M., Kit, E., Wygnanski, I. 1985. Large scale structures in a forced turbulent mixing layer. *J. Fluid Mech.* 150: 23–39

Guyon, E. 1988. Self-sustained oscillations in low density jets. *Intern. Rep.*, Dep. Aerosp. Eng., Univ. South. Calif., Los Angeles

Hannemann, K. 1988. Numerische Simulation und stabilitätstheoretische Untersuchung des absolut und konvectiv instabilen Nachlaufs. *DFVLR Rep. No. FB 88-09*

Hannemann, K., Oertel, H. Jr. 1989. Numerical simulation of the absolutely and convectively unstable wake. *J. Fluid Mech.* 199: 55–88

Heinrich, R., Ahlers, G., Cannell, D. S. 1987. Traveling waves and spatial variation in the convection of a binary mixture. *Phys. Rev. A* 35: 2761–64

Ho, C. M., Huerre, P. 1984. Perturbed free shear layers. *Annu. Rev. Fluid Mech.* 16: 365–424

Huerre, P. 1983. Finite-amplitude evolution of mixing layers in the presence of solid boundaries. *J. Méc. Théor. Appl., Spéc. Iss.*, pp. 121–45

Huerre, P. 1987. Spatio-temporal instabilities in closed and open flows. In *Instabilities and Nonequilibrium Structures*, ed. E.

Tirapegui, D. Villaroel, pp. 141–77. Dordrecht: Reidel
Huerre, P. 1988. On the absolute/convective nature of primary and secondary instabilities. In *Propagation in Systems Far From Equilibrium*, ed. J. E. Wesfreid, H. R. Brand, P. Manneville, G. Albinet, N. Boccara, pp. 340–53. Berlin: Springer-Verlag
Huerre, P., Chomaz, J. M., Redekopp, L. G. 1988. A frequency selection mechanism in spatially-developing flows. *Bull. Am. Phys. Soc.* 33: 2283
Huerre, P., Monkewitz, P. 1985. Absolute and convective instabilities in free shear layers. *J. Fluid Mech.* 159: 151–68
Hultgren, L. S., Aggarwal, A. K. 1987. A note on absolute instability of the Gaussian wake profile. *Phys. Fluids* 30: 3383–87
Inoue, O. 1985. A new approach to flow problems past a porous plate. *AIAA J.* 23: 1916–21
Jackson, C. P. 1987. A finite-element study of the onset of vortex shedding in flow past variously shaped bodies. *J. Fluid Mech.* 182: 23–45
Jackson, T. L., Grosch, C. E. 1989. Absolute/convective instabilities and the convective Mach number in a compressible mixing layer. Submitted for publication
Karniadakis, G. E., Triantafyllou, G. S. 1989. Frequency selection and asymptotic states in laminar wakes. *J. Fluid Mech.* 199: 441–69
Kim, I., Pearlstein, A. J. 1989. Stability of the flow past a sphere. Submitted for publication
Koch, W. 1985. Local instability characteristics and frequency determination of self-excited wake flows. *J. Sound Vib.* 99: 53–83
Koch, W. 1986. Direct resonances in Orr-Sommerfeld problems. *Acta Mech.* 58: 11–29
Kolodner, P., Surko, C. M. 1988. Weakly nonlinear traveling-wave convection. *Phys. Rev. Lett.* 61: 842–45
Kolodner, P., Surko, C. M., Williams, H. 1989. Dynamics of traveling waves near the onset of convection in binary fluid mixtures. *Proc. Conf. Adv. Fluid Turbul., Los Alamos, N.M.* In press
Koochesfahani, M. M., Frieler, C. E. 1987. Instability of non-uniform density free shear layers with a wake profile. *AIAA Pap. No. 87-0047*
Kupfer, K., Bers, A., Ram, A. K. 1987. The cusp map in the complex-frequency plane for absolute instabilities. *Phys. Fluids* 30: 3075–82
Kyle, D. 1988. LIF images of He/N_2 jets. *Mech. Eng. Rep. No. FM88DK1*, Yale Univ., New Haven, Conn.
Kyle, D., Sreenivasan, K. R. 1989. Stability properties of He/air jets. *Proc. ASME Fluids Eng. Spring Conf., La Jolla, Calif.* In press
Landahl, M. T. 1972. Wave mechanics of breakdown. *J. Fluid Mech.* 56: 775–802
Landau, L., Lifshitz, E. M. 1954. *Mechanics of Continuous Media*. Moscow: Fizmatgiz (In Russian)
Landau, L., Lifshitz, E. M. 1959. *Fluid Mechanics*, p. 113. London: Pergamon
Laufer, J., Monkewitz, P. A. 1980. On turbulent jet flows: a new perspective. *AIAA Pap. No. 80-0962*
Lecordier, J. C., Hamma, L., Paranthoen, P. 1988. The control of vortex shedding behind heated circular cylinders at low Reynolds numbers. Submitted for publication
Leib, S. J., Goldstein, M. E. 1986a. The generation of capillary instabilities on a liquid jet. *J. Fluid Mech.* 168: 479–500
Leib, S. J., Goldstein, M. E. 1986b. Convective and absolute instability of a viscous liquid jet. *Phys. Fluids* 29: 952–54
Lifshitz, E. M., Pitaevskii, L. P. 1981. *Physical Kinetics*, Chap. 6. London: Pergamon
Lin, S. J., Pierrehumbert, R. T. 1986. Absolute and convective instability of inviscid stratified shear flows. In *Preprints, Int. Symp. Stratified Flows, Calif. Inst. Technol., Pasadena*, pp. 1–10
Lin, S. P., Lian, Z. W. 1989. Absolute instability of a liquid jet in a gas. *Phys. Fluids* 31: 3260–65
Lowery, P. S., Reynolds, W. C. 1986. Numerical simulation of spatially-developing, forced, plane mixing layer. *Rep. No. TF-26*, Dep. Mech. Eng., Stanford Univ., Stanford, Calif.
Luecke, M., Mihelcic, M., Wingerath, K. 1984. Propagation of Taylor vortex fronts into unstable circular Couette flow. *Phys. Rev. Lett.* 52: 625–28
Luecke, M., Mihelcic, M., Wingerath, K. 1985. Front propagation and pattern formation of Taylor vortices growing into unstable circular Couette flow. *Phys. Rev. A* 31: 396–409
Mack, L. M. 1985. The wave pattern produced by point source on a rotating disc. *AIAA Pap. No. 85-0490*
Mathis, C., Provansal, M., Boyer, L. 1984. The Bénard-von Kármán instability: an experimental study near the threshold. *J. Phys. (Paris) Lett.* 45: 483–91
Mattingly, G. E., Criminale, W. O. 1972. The stability of an incompressible two-dimensional wake. *J. Fluid Mech.* 51: 233–72
Merkine, L. O. 1977. Convective and abso-

lute instability of baroclinic eddies. *Geophys. Astrophys. Fluid Dyn.* 9: 129–57
Michalke, A. 1965. On spatially growing disturbances in an inviscid shear layer. *J. Fluid Mech.* 23: 521–44
Michalke, A. 1970. A note on the spatial jet-instability of the compressible cylindrical vortex sheet. *Rep. DLR-FB 70-51*, Dtsch. Luft- und Raumfarht, Berlin
Michalke, A. 1971. Instabilitaet eines Kompressiblen runden Freistrahls unter Beruecksichtigung des Einflusses der Strahlgrenzschicht Dicke. *Z. Flugwiss.* 19: 319–28
Michalke, A. 1984. Survey on jet instability theory. *Prog. Aerosp. Sci.* 31: 159–99
Mikhailovskii, A. B. 1974. *Theory of Plasma Instabilities*, Vol. 1, Chaps. 4, 5. New York: Consult. Bur.
Monkewitz, P. A. 1988a. The absolute and convective nature of instability in two-dimensional wakes at low Reynolds numbers. *Phys. Fluids* 31: 999–1006
Monkewitz, P. A. 1988b. A note on vortex shedding from axisymmetric bluff bodies. *J. Fluid Mech.* 192: 561–75
Monkewitz, P. A. 1988c. Local and global resonances in heated jets. *Proc. AFOSR Contract. Meet. Res. Turbul., Univ. So. Calif., Los Angeles*, pp. 1–4
Monkewitz, P. A. 1989a. Feedback control of global oscillations in fluid systems. *AIAA Pap. No. 89-0991*
Monkewitz, P. A. 1989b. The role of absolute and convective instability in predicting the behavior of fluid systems. *Proc. ASME Fluids Eng. Spring Conf., La Jolla, Calif.* In press
Monkewitz, P. A., Bechert, D. W., Barsikow, B., Lehmann, B. 1988a. Experiments on the absolute instability of heated jets. *Proc. Eur. Turbul. Conf., 2nd.* In press
Monkewitz, P. A., Bechert, D. W., Barsikow, B., Lehmann, B. 1989a. Self-excited oscillations and mixing in a heated round jet. Submitted for publication
Monkewitz, P. A., Davis, J., Bojorquez, B., Yu, M.-H. 1988b. The breakup of a liquid jet at high Weber number. *Bull. Am. Phys. Soc.* 33: 2273
Monkewitz, P. A., Huerre, P., Chomaz, J. M. 1987. Preferred modes in jets and global instabilities. *Bull. Am. Phys. Soc.* 32: 2051
Monkewitz, P. A., Huerre, P., Chomaz, J. M. 1989b. Preferred modes in two-dimensional jets. In preparation
Monkewitz, P. A., Lehmann, B., Barsikow, B., Bechert, D. W. 1989c. The spreading of self-excited hot jets by side-jets. *Phys. Fluids A* 1: 446–48
Monkewitz, P. A., Nguyen, L. N. 1987. Absolute instability in the near wake of two-dimensional bluff bodies. *J. Fluids Struct.* 1: 165–84
Monkewitz, P. A., Sohn, K. D. 1986. Absolute instability in hot jets and their control. *AIAA Pap. No. 86-1882*
Monkewitz, P. A., Sohn, K. D. 1988. Absolute instability in hot jets. *AIAA J.* 26: 911–16
Mori, Y., Hijikata, K., Nobuhara, T. 1986. A fundamental study of symmetrical vortex generation behind a cylinder by wake heating or by splitter plate or mesh. *Int. J. Heat Mass Transfer* 29: 1193–1201
Morkovin, M. V. 1988. Recent insights into instability and transition to turbulence in open-flow systems. *AIAA Pap. No. 88-3675*
Moses, E., Fineberg, J., Steinberg, V. 1987. Multistability and confined travelling-wave patterns in a convecting binary mixture. *Phys. Rev. A* 35: 2757–60
Moses, E., Steinberg, V. 1986. Flow patterns and nonlinear behavior of travelling waves in a convective binary fluid. *Phys. Rev. A* 34: 693–96
Nakaya, C. 1976. Instability of the near wake behind a circular cylinder. *J. Phys. Soc. Jpn.* 41: 1087–88
Newell, A. C., Whitehead, J. A. 1969. Finite bandwidth, finite amplitude convection. *J. Fluid Mech.* 38: 279–303
Niklas, M., Luecke, M., Mueller-Krumbhaar, H. 1989. Propagating front of a propagating pattern: influence of group velocity. *Europhys. Lett.* 9: 237–42
Noto, K., Ishida, H., Matsumoto, R. 1985. A breakdown of the Kármán vortex street due to the natural convection. In *Flow Visualization III*, ed. W. J. Yang, pp. 348–52. Washington, DC: Hemisphere
Olinger, D. J., Sreenivasan, K. R. 1988. Nonlinear dynamics of the wake of an oscillating cylinder. *Phys. Rev. Lett.* 60: 797–800
Park, D., Huerre, P. 1988. On the convective nature of the Goertler instability. *Bull. Am. Phys. Soc.* 33: 2552
Pavithran, S., Redekopp, L. G. 1989. The absolute-convective transition in subsonic mixing layers. *Phys. Fluids.* In press
Pierrehumbert, R. T. 1984. Local and global baroclinic instability of zonally varying flow. *J. Atmos. Sci.* 41: 2141–62
Pierrehumbert, R. T. 1986. Spatially amplifying modes of the Charney baroclinic-instability problem. *J. Fluid Mech.* 170: 293–317
Pokrovskii, V. L., Khalatnikov, I. M. 1961. On the problem of above-barrier reflection of high-energy particles. *Sov. Phys. JETP* 13: 1207–10
Provansal, M., Mathis, C., Boyer, L. 1987. Bénard-von Kármán instability: transient

and forced regimes. *J. Fluid Mech.* 182: 1–22

Ramshankar, R. 1986. Experiments on a temporal analog of spatially developing free shear flows. *Rep. 86FM-5*, Yale Univ., New Haven, Conn.

Reed, H. L., Saric, W. S. 1989. Stability of three-dimensional boundary layers. *Annu. Rev. Fluid Mech.* 21: 235–84

Reisenthel, P. 1988. *Hybrid instability in an axisymmetric jet with enhanced feedback.* PhD thesis. Ill. Inst. Technol., Chicago

Rockwell, D., Naudascher, E. 1979. Self-sustained oscillations of impinging free-shear layers. *Annu. Rev. Fluid Mech.* 11: 67–94

Scholz, D. 1986. Kohaerente Wirbelstrukturen im Nachlauf einer ruhenden und einer schwingungserregten Kreisscheibe. *Rep. No. DFVLR-FB 86-04*, Berlin

Shraiman, B., Bensimon, D. 1985. On the dynamical mechanism for velocity selection. *Phys. Script.* T9: 123–25

Sreenivasan, K. R. 1985. Transition and turbulence in fluid flows and low-dimensional chaos. In *Frontiers in Fluid Mechanics*, ed. S. H. Davis, J. L. Lumley, pp. 41–67. Berlin: Springer-Verlag

Sreenivasan, K. R., Raghu, S., Kyle, D. 1989a. Absolute instability in variable density round jets. *Exp. Fluids* 7: 309–17

Sreenivasan, K. R., Strykowski, P. J., Olinger, D. J. 1987. Hopf bifurcation, Landau equation and vortex shedding behind circular cylinders. In *Proc. Forum Unsteady Flow Sep.*, ed. K. N. Ghia, 52: 1–13. New York: ASME

Sreenivasan, K. R., Strykowski, P. J., Olinger, D. J. 1989b. On the Hopf bifurcation and Landau-Stuart constants associated with vortex "shedding" behind circular cylinders. Submitted for publication

Steinberg, V., Fineberg, J., Moses, E., Rehberg, I. 1989. Pattern selection and transition to turbulence in propagating waves. *Physica D.* In press

Stewartson, K., Stuart, J. T. 1971. A nonlincar instability theory for a wave system in plane Poiseuille flow. *J. Fluid Mech.* 48: 529–45

Strykowski, P. J. 1986. *The control of absolutely and convectively unstable shear flows.* PhD thesis. Yale Univ., New Haven, Conn.

Strykowski, P. J., Sreenivasan, K. R. 1989. On the formation and suppression of vortex "shedding" at low Reynolds numbers. Submitted for publication

Sturrock, P. A. 1958. Kinematics of growing waves. *Phys. Rev.* 112: 1488–1503

Sturrock, P. A. 1961. Amplifying and evanescent waves, convective and non-convective instabilities. In *Plasma Physics*, ed. J. E. Drummond, pp. 124–42. New York: McGraw-Hill

Subbarao, E. R. 1987. *An experimental investigation of the effects of Reynolds number and Richardson number on the structure of a co-flowing buoyant jet.* PhD thesis. Stanford Univ., Stanford, Calif.

Tam, C. K. W. 1971. Directional acoustic radiation from a supersonic jet generated by shear layer instability. *J. Fluid Mech.* 46: 757–68

Tam, C. K. W. 1978. Excitation of instability waves in a two-dimensional shear layer by sound. *J. Fluid Mech.* 89: 357–71

Tam, C. K. W. 1981. The excitation of Tollmien-Schlichting waves in low subsonic boundary layers by free-stream sound waves. *J. Fluid Mech.* 109: 483–501

Thacker, W. C. 1976. Spatial growth of Gulf Stream meanders. *Geophys. Fluid Dyn.* 7: 271–95

Thorpe, S. A. 1971. Experiments on the instability of stratified shear flows: miscible fluids. *J. Fluid Mech.* 46: 299–319

Triantafyllou, G. S., Dimas, A. 1989. The low Froude number wake of floating bluff objects. *Intern. Rep. No. MITSG 89-5*, Mass. Inst. Technol., Cambridge

Triantafyllou, G. S., Kupfer, K., Bers, A. 1987. Absolute instabilities and self-sustained oscillations in the wakes of circular cylinders. *Phys. Rev. Lett.* 59: 1914–17

Triantafyllou, G. S., Triantafyllou, M. S., Chryssostomidis, C. 1986. On the formation of vortex streets behind stationary cylinders. *J. Fluid Mech.* 170: 461–77

Twiss, R. Q. 1951a. On oscillations in electron streams. *Proc. Phys. Soc. London Sect. B* 64: 654–65

Twiss, R. Q. 1951b. On Bailey's theory of amplified circulating polarized waves in an ionized medium. *Phys. Rev.* 84: 448–57

Twiss, R. Q. 1952. Propagation in electron-ion streams. *Phys. Rev.* 88: 1392–1407

Van Atta, C. W., Gharib, M. 1987. Ordered and chaotic vortex streets behind circular cylinders at low Reynolds numbers. *J. Fluid Mech.* 174: 113–33

Van Atta, C. W., Gharib, M., Hammashe, M. 1988. Three-dimensional structures of ordered and chaotic vortex streets behind circular cylinders at low Reynolds numbers. *Fluid Dyn. Res.* 3: 127–32

Van Saarlos, W. 1988. Front propagation into unstable states: marginal stability as a dynamical mechanism for velocity selection. *Phys. Rev. A* 37: 211–29

Van Saarlos, W. 1989. Front propagation into unstable states II: linear versus nonlinear marginal stability and rate of convergence. Submitted for publication

Walden, R. W., Kolodner, P., Passner, A., Surko, C. M. 1985. Traveling waves and

chaos in convection in binary fluid mixtures. *Phys. Rev. Lett.* 55: 496–99

Wehrmann, O. 1957. Akustische Steuerung der turbulenten Anfachung im Freistrahl. In *Jahrbuch der Wissenschaftlichen Gesellschaft fuer Luftfahrt* (*WGL*), pp. 102–8. Braunschweig: Friedr. Vieweg & Sohn

Wilkinson, S. P., Malik, M. R. 1985. Stability experiments in the flow over a rotating disk. *AIAA J.* 23: 588–95

Williams-Stuber, K., Gharib, M. 1989. Transition from order to chaos in the wake of an airfoil. In press

Wood, C. J. 1964. The effect of base bleed on a periodic wake. *J. R. Aeronaut. Soc.* 68: 477–82

Yang, X., Zebib, A. 1989. Absolute and convective instability of a cylinder wake. *Phys. Fluids A* 1: 689–96

Yu, M.-H., Monkewitz, P. A. 1988. Self-excited oscillations in a low-density two-dimensional jet. *Bull. Am. Phys. Soc.* 33: 2246

Zebib, A. 1987. Stability of viscous flow past a circular cylinder. *J. Eng. Math.* 21: 155–65

Annual Review of Fluid Mechanics
Volume 22, 1990

CONTENTS